A STUDY ON THE COHERENT ATOMIC EFFECTS AND THEIR APPLICATIONS

A Dissertation

by

QINGQING SUN

Submitted to the Office of Graduate Studies of
Texas A&M University
in partial fulfillment of the requirements for the degree of

DOCTOR OF PHILOSOPHY

May 2010

Major Subject: Physics

A STUDY ON THE COHERENT ATOMIC EFFECTS AND THEIR APPLICATIONS

A Dissertation

by

QINGQING SUN

Submitted to the Office of Graduate Studies of
Texas A&M University
in partial fulfillment of the requirements for the degree of

DOCTOR OF PHILOSOPHY

Approved by:

Co-Chairs of Committee,	M. Suhail Zubairy
	Marlan O. Scully
Committee Members,	Alexei Sokolov
	Philip R. Hemmer
Head of Department,	Edward S. Fry

May 2010

Major Subject: Physics

ABSTRACT

A Study on the Coherent Atomic Effects

and Their Applications. (May 2010)

Qingqing Sun, B.S., Peking University;

M.S., Peking University

Co–Chairs of Advisory Committee: Dr. M. Suhail Zubairy
Dr. Marlan O. Scully

Coherent atomic states prepared by laser field can have quantum interference between the different transition amplitudes. Therefore, the medium susceptibility and optical response can be engineered, leading to many interesting phenomena, such as coherent population trapping (CPT), electromagnetically induced transparency (EIT), and lasing without inversion (LWI).

We studied the coherence effects in various prototype atomic systems, and found many interesting applications. We solved the slow light bandwidth problem by decomposing the pulse and matching each frequency to its EIT window using a magnetic field gradient. We also considered the probe field deflection induced by the driving field distribution in EIT, and showed that even a broadband pulse can be deflected without serious spreading. In the fast light area, we examined the effects of noise and parameter deviations in a bichromatic Raman type white light cavity. Taking advantage of the adjustable absorption of EIT, we showed that EIT in a laser cavity can have either first-order or second-order phase transitions. Last but not least, we show that the adiabatic population transfer can be used to reverse the weak measurement of an arbitrary field with finite photon number.

To My Wife Xi Wang and My Parents: Yongshou Sun and Xiumei Zhang

ACKNOWLEDGMENTS

My special thanks go to my advisor, Dr. M. Suhail Zubairy. I learned a lot from his spirit in research and teaching. His ingenious ideas never cease to amaze me and lead to many fruitful results. I also want to thank him for giving me the chance to see the world and meet many collaborators. I would like to thank my co-chair Dr. Marlan O. Scully for his guidance and support throughout my study. His sharp thinking and hard working always inspired me. I also appreciate my committee members, Dr. Philip R. Hemmer, Dr. Alexei Sokolov, and previous member Dr. Yuri V. Rostovtsev for their helpful discussions and collaborations.

Thanks also to my colleagues Dr. M. Al-Amri, Dr. Luiz Davidovich, Dr. Jonathan P. Dowling, Dr. Joerg Evers, Dr. Ali Kamli, Dr. Martin Kiffner, Dr. Hyunchul Nha, Dr. C. H. Raymond Ooi, and Dr. M. Selim Shahriar. Their help was essential in many of the projects. It has been a great pleasure to discuss and learn from them. I also want to extend my gratitude to the department faculty and staff, especially Mrs. Sandi Smith for her help with all these forms and rules.

Last but not least, I thank my friends Gombojav O. Ariunbold, Juntao Chang, Tiegang Di, Hichem Eleuch, Moochan Kim, Hebin Li, Zeyang Liao, Haidong Liu, Jiahui Peng, Eyob A. Sete, Deqiang Sun, Dong Sun, Han Xiong, Shuai Yang, Aihua Zhang, Miaochan Zhi and many more for their help in life and research. Thanks to my mother and father for their encouragement and to my wife Xi Wang for her patience and love.

TABLE OF CONTENTS

CHAPTER Page

I INTRODUCTION 1

A. Semiclassical theory 3
B. Coherent population trapping 5
C. Electromagnetically induced transparency 7

II OPTICALLY CONTROLLED DELAYS FOR BROADBAND PULSES* 10

A. Introduction 10
B. Setup 11
C. Analysis and discussion 13
D. Effects of the EIT medium and the phase shifter 20
E. Conclusion 21

III OPTICAL BEAM STEERING BASED ON ELECTROMAGNETICALLY INDUCED TRANSPARENCY* 22

A. Introduction 22
B. Beam propagation in inhomogeneous medium 23
C. Discussion 26
1. Single frequency deflection 26
2. Focusing and defocusing 31
3. Short pulse deflection 33
D. Conclusion 36

IV ELECTROMAGNETICALLY INDUCED TRANSPARENCY INSIDE THE LASER CAVITY: SWITCH BETWEEN FIRST-ORDER AND SECOND-ORDER PHASE TRANSITIONS* . . 38

A. Introduction 38
B. Free energy for a laser with/without a saturable absorber . 41
C. Derivation and discussion 42
D. Conclusion 50

V EFFECTS OF NOISE AND PARAMETER DEVIATION IN A BICHROMATIC RAMAN TYPE WHITE LIGHT CAVITY* 51

CHAPTER Page

A. Introduction 51
B. Parameter dependence of the susceptibility 53
C. Effect of laser phase and amplitude noise 56
D. Conclusion 61

VI REVERSING THE WEAK MEASUREMENT OF AN ARBITRARY FIELD WITH FINITE PHOTON NUMBER* 62

A. Introduction 62
B. Schemes 63
1. Multi-atom scheme 64
2. Zeeman-level scheme 66
3. Probability and information analysis 68
C. Click-allowed reversal 69
D. Conclusion 73

VII SUMMARY 75

REFERENCES 76

VITA 91

LIST OF FIGURES

FIGURE		Page
1	Interaction between a single mode field and a two-level atom.	4
2	Coherent population trapping in a three-level Λ system.	6
3	Susceptibility curve for the EIT medium.	8
4	Schemes providing a continuous controllable delay to a broadband optical pulse.	11
5	Pulse decomposition and the magnetic field gradient	12
6	Pulse distortion for different drive field intensity	15
7	Piecewise EIT	16
8	The scheme and the susceptibility curve	25
9	Deflection effects for various drive field profiles	27
10	Deflection angle and transmission curves for the profile $\Omega(x) = \Omega_0/\sqrt{1+\beta x}$	29
11	Numerical simulation for beam propagation	30
12	Beam spreading for the profile $\Omega(x) = \Omega_0(1+\beta x)$	31
13	Focusing effect for the profile $\Omega(x) = \Omega_0/\sqrt{1-\beta x^2}$	32
14	Scheme for broadband pulse deflection	34
15	Deflection angle and transmission for the broadband pulse	35
16	The setup of EIT in a laser cavity	43
17	Intensity-Q factor curves for different drive Rabi frequencies	46
18	Phase diagram for the system	48

FIGURE Page

19 Intensity-N_g^e curves for different drive Rabi frequencies 49

20 The scheme of the bichromatic Raman system 53

21 The probe susceptibility of a typical bichromatic Raman system . . . 54

22 The transmission curve of the white light cavity 60

23 The multi-atom scheme 65

24 The Zeeman-level scheme 67

25 The reversal probability and gained information curves 70

26 The state protection probability-time curves for no-click reversal, and click-allowed reversals with $m = 2, 9, 20 (n \equiv m - 1)$. 72

CHAPTER I

INTRODUCTION

Quantum coherence has been a fascinating subject since the birth of quantum mechanics. Adding the probability amplitudes instead of transition probabilities has led to many counterintuitive effects. Laser is a powerful tool to prepare atomic and molecular media into states with quantum coherence. These media exhibit modification of the optical response due to the interference between different excitation paths, which enables various interesting phenomena. One early example is the coherent population trapping (CPT) [1, 2, 3]. In CPT, the two fields pump the atoms into a superposition state called dark state, whose excitation probability amplitude is zero due to the destructive interference between the two paths. So the population is effectively trapped in the dark state. Another closely related phenomenon is electromagnetically induced transparency (EIT) [4, 5, 6], in which the modification of the field is also considered. Since the medium has been prepared into the dark state, ideally they will no longer absorb these resonant fields, hence the name.

EIT has brought a rich set of features in optical response. For example, the steep dispersion around the transparency frequency allows slow light propagation without much absorption. Harris group reported the first experiment in Pb vapor with a group velocity of $c/165$ [7], followed by many other experiments with much slower velocities [8, 9, 10, 11]. By adiabatically reducing the drive field Rabi frequency, it is even possible to fully "stop" an optical pulse [12]. What really happens is that the energy in the pulse has been transferred into the Raman spin excitation and stored in the medium. Slow light, with its controllable delay, has potential application in optical

---

The journal model is *IEEE Transactions on Automatic Control.*

communication. While "stopped" light might be useful in optical storage. Refractive index in the EIT window has also been explored [13]. In a usual EIT medium the refractive index is 1 at resonance. However, by adding incoherent pumping it can be significantly enhanced, which can be used in high precision magnetometry, linewidth compression and frequency stabilization.

In this dissertation we discuss the effects of atomic coherence and interference in a wide range of systems. A central theme of my study is based on EIT. In Chapter II we consider the dispersion of EIT and propose a scheme to realize broadband slow light. In Chapter III we make use of the refractive index in EIT. By engineering the intensity profile of the drive field, the probe field can be deflected or focused. In Chapter IV we show that even the absorption property can be useful. By putting an EIT medium into a laser cavity and controlling the drive field intensity, we can switch between first- and second-order phase transitions. We have also studied other problems like effects of noise and parameter deviations in a bichromatic Raman type white light cavity, and reversing the weak measurement of an arbitrary field with finite photon number.

We use semiclassical theory to study the interaction between quantized atoms and classical field. By solving the optical Bloch equation we can find the density matrix and the system properties. In this chapter we first discuss the theoretical framework [14], and then briefly introduce the concept of CPT, EIT, and some other effects outgrown from them.

A. Semiclassical theory

For a given quantum system, we can determine all the observables if we know the state vector $|\psi\rangle$. The expectation value for an observable A is

$$\left\langle \hat{A} \right\rangle = \langle\psi| \hat{A} |\psi\rangle . \tag{1.1}$$

However, such a pure state is very rare in the real world. Due to the interaction with the environment most systems are in mixed states, in which we only know the probability P_ψ for the system to be in a state $|\psi\rangle$. The statistical average gives us the expectation value

$$\begin{aligned} \left\langle \hat{A} \right\rangle &= \sum_\psi P_\psi \langle\psi| \hat{A} |\psi\rangle = \sum_\psi P_\psi \sum_i \langle\psi| \hat{A} |\phi_i\rangle \langle\phi_i|\psi\rangle \\ &= \sum_i \langle\phi_i| \sum_\psi P_\psi |\psi\rangle \langle\psi| \hat{A} |\phi_i\rangle . \end{aligned} \tag{1.2}$$

Here $|\phi_i\rangle$ is the set of orthonormal basis vectors for the system, which satisfies $\sum_i |\phi_i\rangle \langle\phi_i| = 1$.

We can introduce the density matrix operator $\rho = \sum_\psi P_\psi |\psi\rangle \langle\psi|$ and write the above equation as

$$\left\langle \hat{A} \right\rangle = \sum_i \langle\phi_i| \sum_\psi P_\psi |\psi\rangle \langle\psi| \hat{A} |\phi_i\rangle = \sum_i \langle\phi_i| \rho\hat{A} |\phi_i\rangle = \mathrm{Tr}(\rho\hat{A}). \tag{1.3}$$

So with the knowledge of density matrix we could easily find out the expectation values for a mixed state.

Time derivation on the density matrix operator leads to $\dot{\rho} = \sum_\psi P_\psi(|\dot{\psi}\rangle \langle\psi| + |\psi\rangle \langle\dot{\psi}|)$. After substitution of the Schrodinger equation $|\dot{\psi}\rangle = -\frac{i}{\hbar} H |\psi\rangle$ we obtain

$$\dot{\rho} = -\frac{i}{\hbar} [H, \rho] . \tag{1.4}$$

This is the so called *Liouville* equation, from which we can derive a group of equations

Fig. 1. Interaction between a single mode field and a two-level atom.

for the density matrix elements. After adding the relaxation terms we can solve the equations and find the properties of the system. The diagonal terms are the probability for the atom to be in those energy levels, and non-diagonal terms reflect the coherence between two levels.

As an example, we consider the simplest case of a single mode field interacting with a two-level atom. In Fig. 1, $|a\rangle$ and $|b\rangle$ represent the excited and ground levels of the atom, respectively. They are the unperturbed eigenstates for the atomic Hamiltonian, with the eigenvalues $\hbar\omega_a$ and $\hbar\omega_b$. From the completeness relation $|a\rangle\langle a| + |b\rangle\langle b| = 1$, we obtain

$$H_0 = (|a\rangle\langle a| + |b\rangle\langle b|)H_0(|a\rangle\langle a| + |b\rangle\langle b|) = \hbar\omega_a |a\rangle\langle a| + \hbar\omega_b |b\rangle\langle b| . \tag{1.5}$$

The atom-field interaction Hamiltonian

$$\begin{aligned} H_1 &= -er \cdot E(t) = -e(|a\rangle\langle a| + |b\rangle\langle b|)r(|a\rangle\langle a| + |b\rangle\langle b|) \cdot E(t) \\ &= -(\mu_{ab} |a\rangle\langle b| + \mu_{ba} |b\rangle\langle a|) \cdot E(t), \end{aligned} \tag{1.6}$$

where $\mu_{ab} = \mu^*_{ba} = e\langle a| r |b\rangle$ is the matrix element of the electric dipole moment and $E(t) = E\cos\nu t$ is the field at the atom location.

Substituting the Hamiltonian into the Liouville equation and adding the relax-

ation terms, we have

$$\begin{aligned}
\dot{\rho}_{aa} &= -\gamma_a \rho_{aa} + \frac{i}{\hbar}\left[\mu_{ab} E \rho_{ba} - c.c.\right], \\
\dot{\rho}_{bb} &= -\gamma_b \rho_{bb} - \frac{i}{\hbar}\left[\mu_{ab} E \rho_{ba} - c.c.\right], \\
\dot{\rho}_{ab} &= -(i\omega_{ab} + \gamma_{ab})\rho_{ab} - \frac{i}{\hbar}\mu_{ab} E(\rho_{aa} - \rho_{bb}).
\end{aligned} \tag{1.7}$$

where $\omega_{ab} = \omega_a - \omega_b$ is the atomic level separation, γ_a and γ_b are the population relaxation rate and γ_{ab} is the decoherence rate. In a closed system $\rho_{aa} + \rho_{bb} = 1$, we can solve the density matrix. The macroscopic polarization

$$P(t) = N\left[\rho_{ab}(t)\mu_{ba} + c.c.\right] = \frac{\epsilon}{2} E\left[\chi(\nu) e^{-i\nu t} + c.c.\right], \tag{1.8}$$

where N is the atomic number density. So we know the susceptibility χ can be found through the coherence term. As we all know, the optical response of an atomic medium is described by its susceptibility. The real part of the susceptibility is related to the refractive index, and the imaginary part is related to medium absorption. In this simplest case, when the field is at resonance the absorption has a peak and the dispersion is negative. The atomic population undergoes the Rabi oscillation with the Rabi frequency $\Omega_R = \frac{|\mu_{ba}|E}{\hbar}$.

B. Coherent population trapping

Coherent population trapping was first observed and explained in 1976 [1, 2, 3]. To understand this phenomenon, we consider a three-level Λ system as shown in Fig. 2. The Hamiltonian can be written as

$$\begin{aligned}
H = H_0 + H_1 &= \hbar\omega_a |a\rangle\langle a| + \hbar\omega_b |b\rangle\langle b| + \hbar\omega_c |c\rangle\langle c| \\
&- \frac{\hbar}{2}(\Omega_{R1} e^{-i\phi_1} e^{-i\nu_1 t} |a\rangle\langle b| + \Omega_{R2} e^{-i\phi_2} e^{-i\nu_2 t} |a\rangle\langle c| + H.c.),
\end{aligned} \tag{1.9}$$

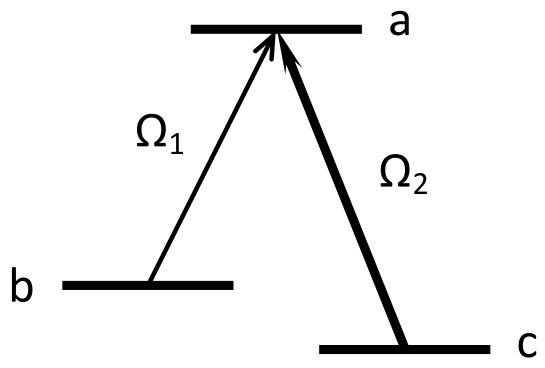

Fig. 2. Coherent population trapping in a three-level Λ system.

in which $\Omega_{R1}e^{-i\phi_1}, \Omega_{R2}e^{-i\phi_2}$ are the complex Rabi frequencies for the two excitation paths.

This Hamiltonian can be simplified in the interaction picture, in which we define

$$U_0(t) = \exp(-\frac{i}{\hbar}H_0 t) = \exp(-i\omega_a t)\left|a\right\rangle\left\langle a\right| + \exp(-i\omega_b t)\left|b\right\rangle\left\langle b\right|. \tag{1.10}$$

The Hamiltonian transforms as

$$\begin{aligned} V(t) &= U_0^{\dagger}(t)H_1U_0(t) \qquad (1.11)\\ &= -\frac{\hbar}{2}\left[\Omega_{R1}e^{-i\phi_1}e^{-i(\nu_1-\omega_{ab})t}\left|a\right\rangle\left\langle b\right| + \Omega_{R2}e^{-i\phi_2}e^{-i(\nu_2-\omega_{ac})t}\left|a\right\rangle\left\langle c\right| + H.c.\right]. \end{aligned}$$

At two-photon resonance $\nu_1 - \omega_{ab} = \nu_2 - \omega_{ac}$, it is easy to find a stationary eigenstate

$$\left|\psi(t)\right\rangle = \frac{\Omega_{R2}e^{-i\phi_2}\left|b\right\rangle - \Omega_{R1}e^{-i\phi_1}\left|c\right\rangle}{\sqrt{\Omega_{R1}^2 + \Omega_{R2}^2}}, \tag{1.12}$$

for which $V\left|\psi(t)\right\rangle = 0$. This state is called dark state because once an atom spontaneously decays into this state, it no longer interacts with the fields. What actually happens is the excitation probability amplitude from the two ground levels cancels with each other. However, an atom in any other state can be excited to level $\left|a\right\rangle$ and has the chance to decay to the dark state. Gradually most of the atoms are trapped

into the dark state.

If instead of constant fields, we adiabatically change the Rabi frequencies, the dark state coefficients will change but the atoms will remain in the dark state. In this way we can adiabatically transfer the population from one component of the superposition state to another component. This process is called stimulated Raman adiabatic passage (STIRAP). For example, by slowly changing from $\Omega_{R2} >> \Omega_{R1}$ to $\Omega_{R2} << \Omega_{R1}$, we can transfer the population from $|b\rangle$ to $|c\rangle$. Since the excited state $|a\rangle$ is never populated during this process, we don't need to worry about spontaneous emission. The transfer efficiency is unity as far as the adiabatic condition is satisfied. Due to these advantages STIRAP has become an important tool to prepare quantum states.

C. Electromagnetically induced transparency

Electromagnetically induced transparency is closely related to CPT. Instead of concentrating on atomic state preparation, in EIT the optical response is also an important part. We consider the same three-level Λ system as in Fig. 2, only now field 1 is a weak probe field and field 2 is a strong coupling field at resonance. The equation of motion for the density matrix can be written as

$$\begin{aligned}
\dot{\rho}_{ab} &= -(i\omega_{ab}+\gamma_{ab})\rho_{ab} - \frac{i\Omega_1 e^{-i\phi_1}e^{-i\nu_1 t}}{2}(\rho_{aa}-\rho_{bb}) + \frac{i\Omega_2 e^{-i\phi_2}e^{-i\nu_2 t}}{2}\rho_{cb}, \\
\dot{\rho}_{cb} &= -(i\omega_{cb}+\gamma_{cb})\rho_{cb} - \frac{i\Omega_1 e^{-i\phi_1}e^{-i\nu_1 t}}{2}\rho_{ca} + \frac{i\Omega_2 e^{i\phi_2}e^{i\nu_2 t}}{2}\rho_{ab}, \\
\dot{\rho}_{ac} &= -(i\omega_{ac}+\gamma_{ac})\rho_{ac} - \frac{i\Omega_2 e^{-i\phi_2}e^{-i\nu_2 t}}{2}(\rho_{aa}-\rho_{cc}) + \frac{i\Omega_1 e^{-i\phi_1}e^{-i\nu_1 t}}{2}\rho_{bc}. \quad (1.13)
\end{aligned}$$

The stationary solution gives us

$$\rho_{ab}(t) = \frac{2i\Omega_1 e^{-i\phi_1}e^{-i\nu_1 t}(-i\Delta+\gamma_{cb})}{4(-i\Delta+\gamma_{ab})(-i\Delta+\gamma_{cb})+\Omega_2^2}, \quad (1.14)$$

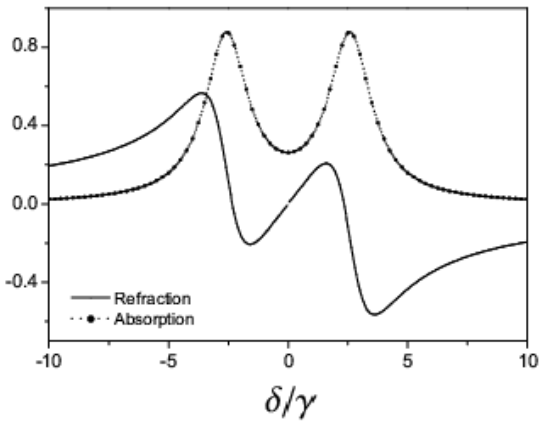

Fig. 3. Susceptibility curve for the EIT medium.

from which we obtain the real part χ' and imaginary part χ''

$$\begin{aligned} \chi' &= -\frac{N|\mu_{ab}|^2\Delta}{\epsilon_0\hbar Z}\left[\gamma_{cb}(\gamma_{ab}+\gamma_{cb})+(\Delta^2-\gamma_{ab}\gamma_{cb}-\frac{\Omega_2^2}{4})\right], \\ \chi'' &= \frac{N|\mu_{ab}|^2}{\epsilon_0\hbar Z}\left[\Delta^2(\gamma_{ab}+\gamma_{cb})-\gamma_{cb}(\Delta^2-\gamma_{ab}\gamma_{cb}-\frac{\Omega_2^2}{4})\right], \end{aligned} \tag{1.15}$$

where $\Delta=\nu_1-\omega_{ab}$ is the probe detuning and $Z=\Delta^2(\gamma_{ab}+\gamma_{cb})^2+(\Delta^2-\gamma_{ab}\gamma_{cb}-\Omega_2^2/4)^2$.

From the susceptibility curve in Fig. 3 we can see the transparency window. Physically the coupling field and the probe field prepare the atomic medium into the dark state. Then the following probe field will not be absorbed. However, due to the decoherence γ_{cb}, atoms can move out of the dark state, causing residue absorption. Since the coupling field is strong, the two absorption peaks are located at $\pm\Omega_2/2$ so the transparency window has the width Ω_2.

The steep positive dispersion in EIT transparency window can be used to propagate slow light. If we send in a pulse whose frequency range is within the EIT window, it will propagate almost losslessly. The group velocity

$$v_g=\frac{d\omega}{dk}=\frac{c}{n+\omega(dn/d\omega)}. \tag{1.16}$$

Typically in an atomic gas medium, the susceptibility is much less than 1. So the refractive index $n = \sqrt{1+\chi'} \approx 1 + \chi'/2$. Substituting into the above equation we have

$$v_g = \frac{c}{1 + \frac{\chi'}{2} + \frac{\omega}{2}\frac{d\chi'}{d\omega}}. \tag{1.17}$$

At the probe resonance $\chi' = 0$ and the slope $d\chi'/d\omega$ is positive, which means slow light. Substitution of the χ' expression shows that approximately $v_g \propto \Omega_2^2$ when the drive field is strong. In order to get ultraslow light we have to lower the drive field intensity, which limits the pulse bandwidth. We show a solution to this problem in Chapter II.

CHAPTER II

OPTICALLY CONTROLLED DELAYS FOR BROADBAND PULSES*

A. Introduction

Recent progress in the study of ultra-short optical pulse generation [15] creates a fundamentally new realm of laser applications in many areas, including material science, information processing, communication and spectroscopy. The rapidly developing technology of broadband optical pulse shaping requires systems to provide controllable delays for such pulses. For example, an optical buffer [16, 17] can be characterized by the maximum number of bits N_b that can be simultaneously stored in the buffer.

In this chapter, we show that the steep dispersion of an EIT medium [4, 14] can be used to create large controllable delays for ultra-short pulses by using the system shown in Fig. 4, thus yielding a large time-delay-bandwidth product. The best product achieved so far in slow-light experiments is 3 [9, 10, 11, 18, 19, 20]. An important feature of our scheme is that the delay is continuously controllable by an optical field. The idea is to synthesize dispersion of the system by using the highly steep dispersion of a three-level atomic system with inhomogeneous broadening.

---

*Part of this chapter is reprinted with permission from "Optically controlled delays for broadband pulses" by Q. Sun, Y. V. Rostovtsev, J. P. Dowling, M. O. Scully, and M. S. Zubairy, 2005. *Phys. Rev. A*, vol. 72, pp. 031802(R), Copyright [2005] by the American Physical Society.

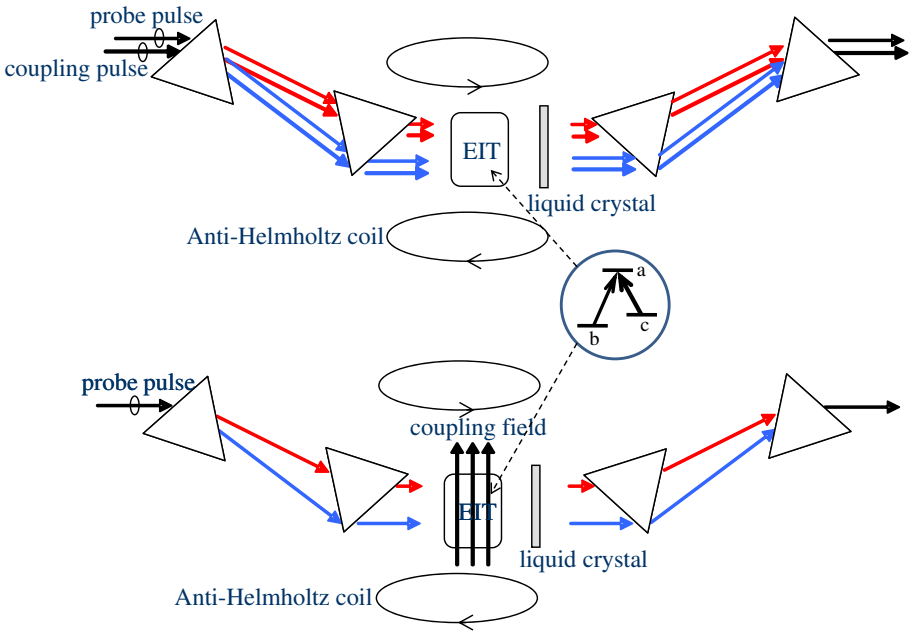

Fig. 4. Schemes providing a continuous controllable delay to a broadband optical pulse.

B. Setup

In Fig. 4 we present two possible schemes. The system consists of a set of prisms (or diffraction gratings) with total dispersion equal to zero. The first prism disperses the probe pulse transforming the parallel beam into divergent beams. The angle of refraction of the light beam with frequency ω_L is $\beta(\omega_L) = [n(\omega_L) - 1]\alpha$ [21], where $n(\omega_L)$ is the refractive index of the material of the prism (see Fig. 5A). The second prism produces parallel beams with different frequencies shifted in space (see Fig. 5A,B). The light beams of varying frequencies then pass through an atomic medium that has an inhomogeneous magnetic field gradient (see Fig. 5C). The medium consists of a three-level atomic system. A drive field couples the levels a and c and the probe field couples levels a and b.

In the first scheme, we maintain one- and two-photon resonances of the drive

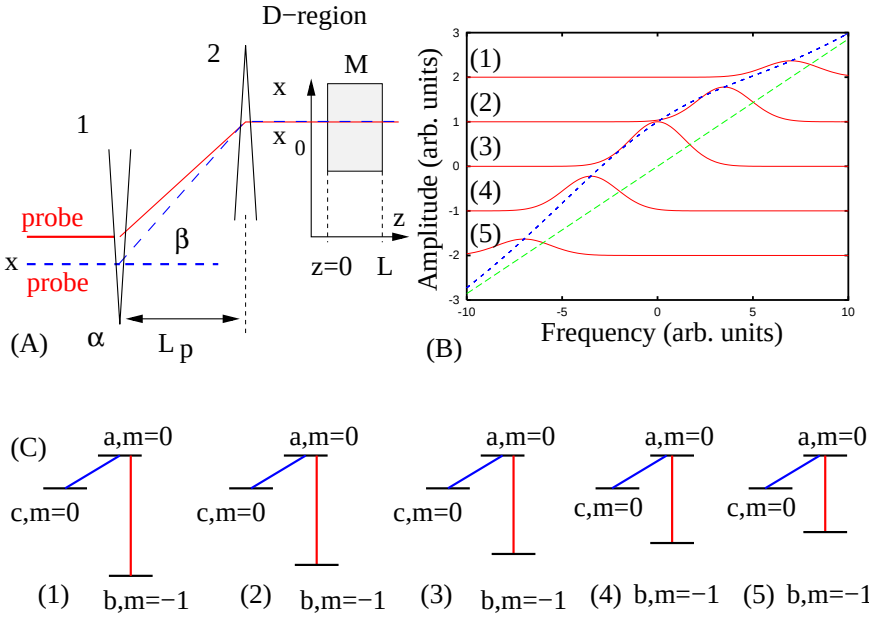

Fig. 5. Pulse decomposition and the magnetic field gradient. (A) The beam of light has a Gaussian profile along x axis. Each ray in the dispersion region consists of all frequencies ω_x that come from the transverse rays dispersed by the prisms. The solid line corresponds to the center of the probe beam, the dashed line is shifted at the distance x from the center of the beam. The D-region is the dispersive region where different frequencies of the probe pulse are separated. (B) The spectra of the probe pulse are shown in different locations of the D-region (1-5). The dash lines show the positions of the maximum and the maximum amplitudes of the probe pulses correspondingly, visualizing the spectral distribution of the probe pulse along x-axis. The total width of the spectra is determined by the duration of the probe pulse. The spectral width of the probe pulse at a particular location is determined by the frequency dispersion of the system of prisms. (C) A three-level atomic medium with inhomogeneous magnetic field. It is shown that at different locations inside medium (1-5) the probe transition has different frequency, $\omega_{ab} = \omega_{ab0} + \alpha x$, that are in resonance with the corresponding frequency component of the probe field, $\omega_L = \omega_0 + \beta x$, via the system of prisms shown in Fig. 4.

and probe fields at the a-c and a-b transitions, respectively, by an appropriate design of the prism system. This scheme can work for hot gases with Doppler broadened transitions. The second scheme has a drive field that propagates in the perpendicular direction to the probe field. Here the medium should not have Doppler broadening, i.e., this scheme works for cold atoms. Also it assumes that the a-c transition is not influenced by the magnetic field at all locations inside the medium, and the drive field is always at resonance (see Fig. 5C). A similar scheme has been presented in [22] and a scheme based on photorefractive materials has also been discussed in [23].

C. Analysis and discussion

We assume a weak probe and a strong resonant drive field, i.e., all population is in state b. The susceptibility χ associated with the a-b transition has the form [14]

$$\chi(\nu_p) = \frac{\eta\gamma(\Delta_p + i\gamma_{cb})}{(\gamma_{cb} - i\Delta_p)(\gamma_{ab} - i\Delta_p) + \Omega^2}, \tag{2.1}$$

where $\Delta_p = \nu_p - \omega_{ab}$ is the detuning of the probe from the atomic transitions a-b; ν_p is the frequency of the probe field E_p; Ω is half of the drive Rabi frequency on the a-c transition, γ_{ab} and γ_{cb} are the decay rates of the atomic coherences ρ_{ab} and ρ_{cb}, respectively; γ is the radiation decay between a and b, and $\eta = 3\lambda^3 N/8\pi^2$ with λ being the wavelength of the probe field and N being the atomic number density. The above equation is just a rewriting of (1.15) for simplicity of the expressions in this Chapter. In hot gases, the Doppler shift changes the detuning $\Delta_p \to \Delta_p + kv$ (k is the wavevector) due to thermal motion. For the sake of simplicity we consider a Lorentzian profile with Doppler width D for the inhomogeneously broadened line shape $F(v)$. Averaging over inhomogenous distribution, i.e., $\langle\chi\rangle_v = \int_{-\infty}^{\infty} dv\chi F(v)$,

gives

$$\chi(\nu_p) = \frac{\eta\gamma(\Delta_p + i\gamma_{cb})}{(\gamma_{cb} - i\Delta_p)(\gamma_{ab} + D - i\Delta_p) + \Omega^2}. \tag{2.2}$$

The real part of χ is given by

$$\chi' = \frac{\eta\gamma\Delta_p(\Omega^2 - \gamma_{cb}^2 - \Delta_p^2)}{(\Omega^2 + \gamma_{cb}D + \gamma_{cb}\gamma_{ab} - \Delta_p^2)^2 + \Delta_p^2(\gamma_{cb} + \gamma_{ab} + D)^2}. \tag{2.3}$$

In general, a pulse propagating in the resonant medium is distorted because χ' has nonvanishing higher-order derivatives with respect to ν_p, and the group velocity for the different frequency components of a pulse are different. We first address the question: What is the largest delay and the shortest pulse that can propagate through this EIT medium without distortion? This question was discussed in Refs. [24, 25]. We shall then analyze the advantages of inhomogeneous magnetic field induced inhomogeneous broadening.

It is clear from (2.3) that the group velocity is positive if $\Omega > 1/T$, where T is the duration of the pulse. Thus, in order to have a delay of the probe pulse, a necessary condition is $\Omega T > 1$.

In order to see the distortion of pulses propagating through the EIT medium, we consider the propagation of a Gaussian probe pulse $\Omega_p(t, z)$, whose spectrum is also Gaussian, i.e.,

$$\Omega_p(t, z = 0) = \Omega_{p0} \exp[-\frac{t^2}{2T^2}], \quad \Omega_p^\omega = \frac{T\Omega_{p0}}{\sqrt{2\pi}} \exp[-\frac{T^2\omega^2}{2}]. \tag{2.4}$$

The wavenumber at frequency ν_p is given by

$$k(\nu_p) = \frac{\nu_p}{c}\sqrt{1 + \chi(\nu_p)} \simeq \frac{\nu_p}{c}[1 + \frac{\chi(\nu_p)}{2}], \tag{2.5}$$

and the probe pulse at the distance z can be calculated by

$$\Omega_p(t, z) = \frac{T\Omega_{p0}}{\sqrt{2\pi}} \int_{-\infty}^{+\infty} d\omega \exp[-i\omega t - \frac{T^2\omega^2}{2} + ik(\omega)z] \tag{2.6}$$

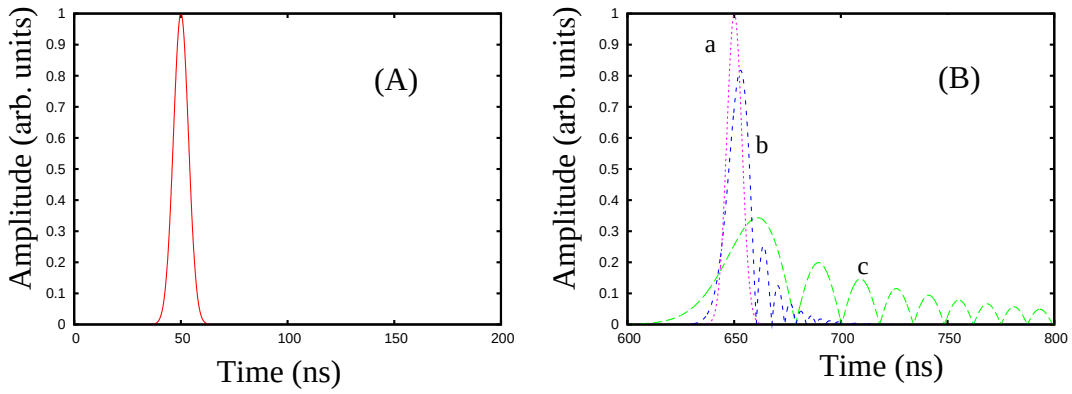

Fig. 6. Pulse distortion for different drive field intensity. (A) Input pulse ($T = 5$ ns) is shown. (B) Delay time $\tau_{delay} = k\eta\gamma L/\Omega^2 = 0.65$ μs. The output pulses correspond to incoming: (a) $\Omega T = 5$, (b) $\Omega T = 25$, (c) $\Omega T = 100$.

For large enough Rabi frequencies the atomic susceptibility is given by

$$\chi'(\nu_p) \simeq \frac{\eta\gamma\Delta_p}{\Omega^2}. \tag{2.7}$$

Therefore, at a position z, the delayed probe pulse is given by

$$\Omega_p(t,z) = \Omega_{p0}\exp[-\frac{(t-z/v_g)^2}{2T^2}], \tag{2.8}$$

where the group velocity of the optical pulse is $v_g \simeq 2\Omega^2/k\eta\gamma$ (see [20]), and the delay time is given by $\tau_{delay} = L/v_g = k\eta\gamma L/2\Omega^2$. Taking into account that $\Omega T > 1$, a good estimate for the delay time is

$$\tau_{delay} < k\eta L\gamma T^2/2. \tag{2.9}$$

Thus a high intensity drive field is needed to obtain significant delay for short pulses (see Fig. 6).

For substantial delay times, the atomic number density should also be large. For

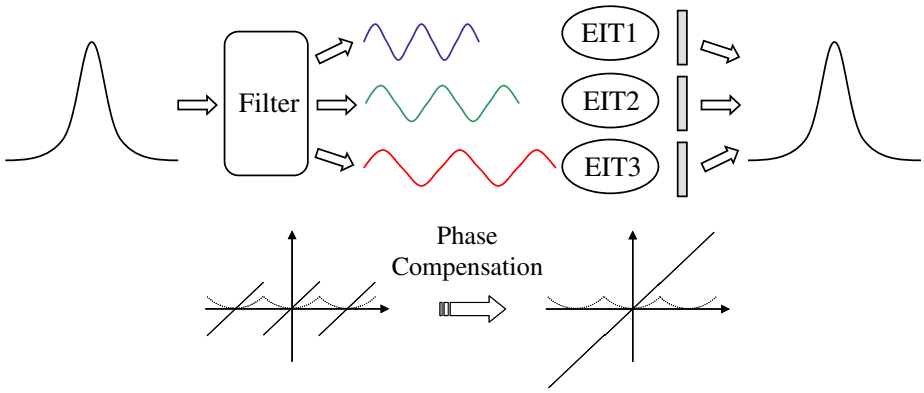

Fig. 7. Piecewise EIT. (top) A broadband pulse is decomposed into several bands and each passes through its own EIT. (bottom) The susceptibility curves for piecewise EIT.

$N = 10^{14}$ cm^{-3}, $L = 1$ cm, $\lambda \simeq 1$ μm, we obtain

$$\tau_{delay} < 10^{12} T^2. \tag{2.10}$$

Thus, for $T = 10^{-9}$ s, the delay time is of the order of a few μs, but for $T = 1$ ps, the delay time is just 1 ps. We also note that the required power for the picosecond time scale is six orders of magnitude higher than that for nanosecond pulses.

To break this bandwidth limit, we can split the broadband pulse into several narrow frequency bands. Each band passes through its own EIT medium. With appropriate phase compensation these bands recombine into a delayed pulse, as shown in the top part of Fig. 7. The bottom part of that Figure shows the susceptibility curves. The dispersion curves for these bands are lined up by the phase compensation. The result is a broad EIT window with steep dispersion, which allows broadband slow light.

To extend this technique to shorter time scales we suggest the setup shown in Fig. 4. Due to the spectral dispersion of the prisms, the probe beam has an angular spread after the first prism. The second prism has the same frequency dispersion,

but its dispersion has the opposite sign relative to the first one. Thus after the second prism the optical beam components become parallel and there is a one-to-one correspondence between the x position and the frequency of the probe and drive fields. As discussed earlier, the inhomogeneous magnetic field shifts the atomic levels such that the probe and the drive fields are in both one-photon and two-photon resonances for atoms at all locations inside the medium. In the limit of infinite spectral resolution, prisms separate different frequencies of the input pulse, and then these frequencies propagate through the EIT medium. For each frequency, the EIT medium produces a time delay given by L/v_g. This results in the delay for the whole pulse which is restored after the second pair of prisms (see Fig.4). The important improvement due to this scheme is that we relax the condition on the strength of the drive field whose role is limited to providing only EIT for a particular frequency. There is no requirement on the drive field to provide a linear dispersion for the range of frequencies corresponding to the pulse spectrum.

However, in practice there is not infinite resolution of frequencies at the input plane $z = 0$. Instead, due to the prism dispersion, there is a frequency distribution at each point on the input plane whose width is of course considerably lower than the spectral width of the original pulse. We next calculate the spectral width of the field at a given point in the input plane (after passage through the double prisms system of Fig. 4).

We assume, for simplicity, that the input pulse has a Gaussian spatial distribution of width d perpendicular to the direction of propagation, as well as a Gaussian time profile corresponding to its duration T, i.e.,

$$\Omega_p(t, x, z = 0) = \Omega_{p0} \exp[-\frac{t^2}{2T^2} - \frac{x^2}{2d^2}]. \tag{2.11}$$

As shown in Fig. 5A, the field at an arbitrary location x_0, corresponding to frequency

ω_0 in the plane $z = 0$, is obtained from a spatial distribution of the original pulse before the first pair of prisms. The field of frequency ω_x coming from the x position of the input pulse at x_0 is related to ω_0 via $x = \alpha L_p \frac{dn(\omega_0)}{d\omega_0}(\omega_x - \omega_0)$, where L_p is the distance between the first two prisms [21] (see Fig. 5). The time dependence of the pulse at the location x_0 is given by adding all frequencies over the transverse distribution of the beam. In Fig. 5, we show five positions in the D-region, the laser pulse at each position has a central frequency and some spread of frequencies that comes from the distribution of the optical beam in the x-direction. Then the probe pulse at a location x_0 with central frequency ω_0 is given by

$$\begin{aligned} \Omega_{\omega_0} &= \frac{T\Omega_{p0}}{\sqrt{2\pi}} \int d\omega_x \times \exp[-(\tau^2(\omega_x - \omega_0)^2 + T^2\omega_x^2)/2 - i\omega_x t] \\ &= \frac{T\Omega_{p0} \exp[-(T^2\tau^2\omega_0^2 - t^2 - 2i\omega_0\tau^2 t)/2(T^2 + \tau^2)]}{\sqrt{T^2 + \tau^2}} \end{aligned} \tag{2.12}$$

where we have introduced $\tau^2 = \alpha^2 L_p^2 (dn(\omega_0)/d\omega_0)^2/d^2$. It is clear that, in the limit $d \to 0$, we have $\tau \to \infty$ and this corresponds to infinite spectral resolution.

Thus, in the dispersion region, the pulse at a given frequency ω_0 has a time duration $\sqrt{T^2 + \tau^2}$ where τ is related to the dispersion of the prism's system β'. After passing through the EIT medium each pulse at a given frequency experiences a delay $\tau_d = L/v_g$, if the Rabi frequency of the drive field satisfies $\Omega\sqrt{T^2 + \tau^2} \simeq \Omega\tau \gg 1$ instead of $\Omega T \gg 1$. Here we see that the prism arrangement allows us to substantially relax the condition on the drive field.

On combining all the frequency components after passage through the medium, we therefore reproduce a short pulse with duration equal to initial time duration T but shifted by τ_d, i.e.,

$$\Omega_p(t, z) = \int d\omega_0 \Omega_p(t - \tau_d, x_0, z) = \Omega_{p0} \exp[-\frac{(t - \tau_d)^2}{2T^2}]. \tag{2.13}$$

We note that different frequency components will acquire linear and nonlinear phase shifts while passing through the EIT medium and an appropriate phase shifter such as liquid crystal will be required to compensate these phase shifts.

The duration of the pulse is determined by the spectral width, which is determined by the inhomogenous broadening that we introduce via the inhomogeneous magnetic field. We note that, locally, the medium is always resonant with the probe and drive fields. The delay time is determined by the density of atoms

$$\tau_{delay} = \frac{L}{v_g} = \frac{k\eta\gamma L}{2\Omega^2} < k\eta L\gamma(T^2 + \tau^2)/2. \tag{2.14}$$

So now even for a short pulse with a small T, it is possible to have a large delay due to the inclusion of τ. There should be no absorption if $\Omega >> 1/\tau$. In addition, for short pulses having a broad spectrum there is a requirement on the magnetic field. That is one needs to create the magnetic field with a gradient matching the dispersion in the prism system at each position in the D-region of the probe field is at resonance. The total shift of the atomic level should correspond to the spectrum of the short pulse $\Gamma = 1/T$. This introduces the condition on the atomic configuration, namely the level b should be able to move linearly with the magnetic field. For example, this condition can be met in Ca atom where the states P_0, P_1, separated by 52 cm^{-1}, and the excited state S_1 form the three-level Λ configuration suitable for our purposes. Thus, for a 10 ps pulse, the change of the magnetic field needs to be about 1 T per atomic cell. This gradient can be created by using just a simple wire with electric current $I = 10^2$ kA (the cell has length $l = 10$ cm and one side of the cell is at the distance of $r_1 = 1$ cm from the wire and the second side at $r_2 = 11$ cm), or using anti-Helmholtz coils.

D. Effects of the EIT medium and the phase shifter

In the piecewise EIT scheme, the EIT medium and the phase shifter work together to produce the delay. However, in the continuous EIT scheme, the EIT medium only provides a large delay for each local pulse. But the global dispersion is zero because each frequency has the same detuning to its local EIT center. It is the phase shifter that introduces a global dispersion and the delay for the short pulse. Naturally one would raise the question, what is the role of EIT here?

To answer this question, we need to analyze the phase delay in the system. After passing through the phase shifter, a frequency component ω at position x would have the phase delay

$$\varphi(\omega, x) = \frac{n(\omega, x)\omega L}{c} + \phi(x) = \left[1 + \alpha'(\Delta\omega - \Delta x \frac{d\omega}{dx})\right] \frac{\omega L}{c} + \Delta x \frac{d\phi}{dx}, \tag{2.15}$$

where $\alpha' = N|\wp|^2/2\varepsilon_0\hbar\Omega^2$, $\Delta\omega = \omega - \omega_c$ is the detuning from the central frequency of the whole pulse, and $\Delta x = x - x_c$ is the displacement from the central ray. For each single frequency, the deflection angle θ is given by

$$\sin\theta = \frac{c}{\omega} \left.\frac{d\varphi}{dx}\right|_{\text{constant } \omega} = \frac{c}{\omega}(-\frac{\alpha'\omega L}{c}\frac{d\omega}{dx} + \frac{d\phi}{dx}). \tag{2.16}$$

So both the EIT medium and the phase shifter have the deflection effect. To avoid the deflection, we set the phase shifter in such a way that the two contributions cancel with each other,

$$\frac{\alpha'\omega L}{c}\frac{d\omega}{dx} = \frac{d\phi}{dx}. \tag{2.17}$$

On the other hand, the global dispersion is related to frequency components spread out from a single ray. For a matching magnetic field gradient, $\Delta\omega - \Delta x d\omega/dx$ is a

constant. So the global delay is

$$\tau_{delay} = \left.\frac{d\varphi}{dx}\right|_{\text{constant } \Delta\omega - \Delta x \frac{d\omega}{dx}} - \frac{L}{c} = \frac{dx}{d\omega}\frac{d\phi}{dx} = \frac{\alpha'\omega L}{c}. \tag{2.18}$$

The global delay solely comes from the phase shifter. Its value is equal to those local delays inside the EIT medium.

So indeed the EIT medium has no contribution to the global dispersion. It cancels out the deflection side effect of the phase shifter.

E. Conclusion

In conclusion, we have suggested and theoretically analyzed a system that can potentially provide delays for broadband optical pulses. Applications of these results hold substantial promise ranging from radar systems and femtosecond pulse shaping techniques to quantum storage for photons having very short coherence times.

CHAPTER III

OPTICAL BEAM STEERING BASED ON ELECTROMAGNETICALLY INDUCED TRANSPARENCY*

A. Introduction

Optical beam deflection is an important technology in modern optics. It has applications in the field of radar, optical imaging, laser machining and free space communication. Many physical mechanisms have been used to obtain the deflection [26, 27]. Among them mechanical motion [28, 29, 30] is the simplest and most convenient way, since it only mechanically moves or rotates the deflector (mirror, grating, etc.). Thermal gradient [31], acoustooptical interaction [32, 33], and electrooptic effect [34, 35, 36] all can induce a refractive index gradient which deflects the light. And the electrooptic deflectors are faster than their acoustooptic counterparts as compared in a 70s review [37]. Nowadays with the development of new materials and devices, the attention has been focused on using photonic crystals [38, 39] and phased arrays [40, 41, 42] to get fast beam steering.

Light can also change the propagation direction of another light through interaction with matter. Beam deflections have been reported in sodium vapor via optical pumping [43] and in rubidium vapor via saturated absorption and hyperfine pumping [44]. Electromagnetically induced transparency (EIT) provides another mechanism since the probe has a steep dispersion near the transparency center [4, 45, 46]. Moseley

*Reprinted with permission from "Optical beam steering based on electromagnetically induced transparency" by Q. Sun, Y. V. Rostovtsev, and M. S. Zubairy, 2006. *Phys. Rev. A*, vol. 74, pp. 033819, Copyright [2006] by the American Physical Society.

et al. first observed the electromagnetically induced focusing and defocusing effects in a rubidium vapor [47, 48], which come from the spatial Gaussian distribution of the drive field. They included both refraction and absorption modification in the numerical calculation and found a qualitatively accordance with the experiment. Mitsunaga et al. observed the absorption imaging in cold sodium atoms [49]. The probe is mostly absorbed after the atom cloud except for the focal point of the drive beam. Transmission through this EIT point can reach almost 200% which is obviously a focusing feature. Another example based on EIT is electromagnetically induced waveguiding [50, 51, 52] which uses the drive field as a fiber to confine the probe field.

In this chapter we explore the possibility and limit of beam deflection through EIT effect. Inhomogeneous drive field intensity produces refractive index gradient for the probe. Ray optics is adopted to analyze the steering angle and absorption for each probe ray. Under optimal distribution, rays of the same frequency can deflect with the same angle, unaffected by the starting position. For single frequency we can also obtain exact focusing. Finally we show that even a whole beam with spatial and spectrum width can be deflected together using a specific setup.

B. Beam propagation in inhomogeneous medium

The idea of an all-optical steering of an electromagnetic wave is as follows. Consider a pulse of central frequency ω propagating through a three-level EIT medium as shown in Fig. 8. We assume that the spectral width of the pulse lies well within the EIT window such that the inequalities $\Omega, \gamma >> \Delta\omega$ are satisfied. Here Ω is the Rabi frequency of the drive field resonant with $a-c$ transition, γ is the atomic decay rate, and $\Delta\omega = \omega - \omega_{ab}$ is the detuning of the probe frequency ω with the atomic transition $a-b$. Now in order to steer the incident pulse to a different direction, we introduce

the phase shift for the different transverse positions x of the pulse at the output by modulating the Rabi frequency of the drive field. Thus the whole pulse has a different direction while coming out of the EIT medium. Here we derive a simple expression for the beam steering angle and the corresponding losses.

We assume that we have a highly dispersive medium. For a large enough Ω, the index of refraction for probe field can be written as

$$n' \simeq 1 + \frac{\chi'}{2} \simeq 1 + \alpha\Delta\omega, \tag{3.1}$$

where N is the atomic density and $\alpha = N|\wp|^2/2\varepsilon_0\hbar\Omega^2$ with $\wp$ being the atomic dipole moment on the a-b transition. Inhomogeneous $\Omega(x)$ leads to inhomogeneous $n'(x)$.

The trajectory of the light rays propagating in an inhomogeneous medium can be found by using the eikonal approximation [21]. We start with the Maxwell's equation that describes the propagation of the electromagnetic waves,

$$\nabla^2 E - \frac{1}{c^2}\frac{\partial^2 E}{\partial t^2} = \mu_0 \frac{\partial^2 P}{\partial t^2}. \tag{3.2}$$

We can expand the field and the polarization in terms of the slowly varying amplitudes E_ν and P_ν and the eikonal ψ as

$$E = \sum_\nu E_\nu e^{-i\nu t + ik\psi}, \quad P = \sum_\nu P_\nu e^{-i\nu t + ik\psi}. \tag{3.3}$$

Here $k = \nu/c$. The polarization of the medium is related to the field intensity as $P_\nu = \epsilon_0\chi_\nu E_\nu$, where the susceptibility is $\chi_\nu = \chi'_\nu + i\chi''_\nu$. If we neglect the second order derivative over coordinates for the amplitude E_ν, the eikonal equation is given by

$$(\nabla\psi)^2 = 1 + \chi'_\nu \simeq n'^2. \tag{3.4}$$

So we can write down $\nabla\psi = n' d\mathbf{R}/ds$ and obtain the geometrical optics differ-

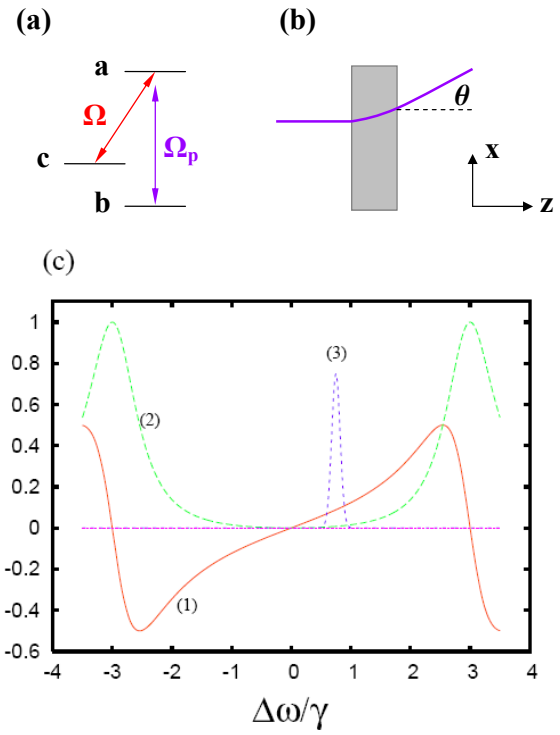

Fig. 8. The scheme and the susceptibility curve. (a) The schematics of a three-level atomic system with the drive fields. (b) A slab of the three-level atomic medium turns a probe light via an inhomogeneous drive field. (c) The real (1) and the imaginary (2) parts of the atomic susceptibility, and the spectrum of probe pulse (3) vs the probe frequency.

ential equation in the vector form

$$\frac{d}{ds}\left(n'\frac{d\mathbf{R}}{ds}\right) = \nabla n', \tag{3.5}$$

where $\mathbf{R}$ is the the point of the ray. Here $\mathbf{R}(x,z) = X(z)\hat{x} + z\hat{z}$ and $\hat{x}$, $\hat{z}$ are the unit vectors along the axes. Then, for the x and z components,

$$\frac{d}{ds}\left(n'\frac{dX}{ds}\right) = \frac{\partial n'}{\partial x}, \text{ and } \frac{d}{ds}\left(n'\frac{dz}{ds}\right) = \frac{\partial n'}{\partial z}. \tag{3.6}$$

The equation describing the amplitude of the electromagnetic field can be obtained in a similar manner. It follows from the imaginary part of (3.2) that

$$2k\nabla\psi\nabla E_\nu + k(\nabla^2\psi)E_\nu = -\frac{\nu^2}{c^2}\chi'' E_\nu. \tag{3.7}$$

The solution of the above equation has the following form

$$E_\nu = \frac{E_{0\nu}}{\sqrt{n'}}\exp\left(-\int_{s_1}^{s_2}\frac{\nu\chi''_\nu}{2n'c}ds\right). \tag{3.8}$$

In the next section we will discuss several inhomogeneous drive field distributions and their steering effects.

C. Discussion

1. Single frequency deflection

For the first case assume that

$$\Omega(x) = \Omega_0/\sqrt{1+\beta x}, \tag{3.9}$$

where β is the parameter that determines the inhomogeneous distribution of the drive field. The refractive index is therefore of the form $n'(x) \simeq 1 + \alpha_0\Delta\omega(1+\beta x)$ with $\alpha_0 = N|\wp|^2/2\varepsilon_0\hbar\Omega_0^2$. This form leads to constant $\nabla n'$ for a single frequency. In the

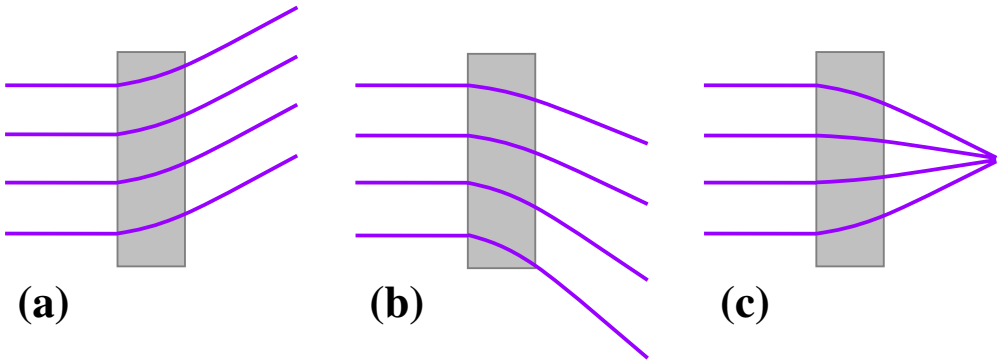

Fig. 9. Deflection effects for various drive field profiles. For different profiles of the drive field the different regimes of probe light propagation takes place. (a) The light deflection angle is the same for all the light rays; (b) the probe light turns but spreads; (c) the focusing of the probe.

following we show that, for such a situation, we obtain the same steering angle for all the transverse position x as shown in Fig. 9a. If the dependence of the drive field has a different form then there will be a spread of the optical rays as shown in Fig. 9b.

In (3.6) using $ds = \sqrt{dX(z)^2 + dz^2}$ and $n' = 1 + \alpha_0 \Delta\omega(1 + \beta x)$, we obtain

$$\frac{d}{ds}\left(n'\frac{dX}{ds}\right) = \alpha_0 \Delta\omega\beta, \quad \text{and} \quad \frac{d}{ds}\left(n'\frac{dz}{ds}\right) = 0. \tag{3.10}$$

The ordinary differential equation to describe the ray trajectory is given by

$$\frac{d^2X(z)}{dz^2} = \frac{1 + \alpha_0\Delta\omega(1 + \beta X(z))}{[1 + \alpha_0\Delta\omega(1 + \beta X_0)]^2}\alpha_0\Delta\omega\beta \simeq \alpha_0\Delta\omega\beta, \tag{3.11}$$

and its solution is

$$X(z) \simeq X_0 + \frac{\alpha_0\Delta\omega\beta z^2}{2}. \tag{3.12}$$

The light turning angle θ can be found from $dX(z)/dz = \tan\theta \simeq \theta$. The resulting angle is

$$\theta \simeq \alpha_0\Delta\omega\beta L = \frac{N|\wp|^2}{2\varepsilon_0\hbar\Omega_0^2}\Delta\omega\beta L. \tag{3.13}$$

Calculation based on full expression of χ [14] shows these simple estimations (3.12,3.13) are valid for small deflection. Under parameters $\beta = 5000/m, L = 1cm, \Omega_0 = 50\pi MHz, N = 10^{15}/cm^3, \lambda = 0.5\mu m, \gamma_{ab} = \gamma_{rad} = 2\pi MHz, \gamma_{cb} = 1kHz$ we get Fig. 10. A probe beam with detuning $\Delta\omega = 3.3MHz$ (Fig. 10a,b) will experience the same deflection angle 5.76°, although the ray starting position X_0 ranges from 0 to 0.2mm. The transmission decreases at larger X_0 because there Ω is smaller. Fig. 10(c,d) shows the linear dependence of deflection angle to detuning. Now X_0 is fixed at 0 and $\Delta\omega$ varies from $-4MHz$ to $4MHz$. The transmission at negative $\Delta\omega$ is larger because the ray goes to negative x direction where Ω is larger.

To study the behavior of a beam with a finite diameter we perform some numerical simulation. Consider a monochromatic electromagnetic wave with frequency ω, the Helmholtz equation is given by

$$\nabla^2\mathbf{E} + 2\nabla(\mathbf{E}\cdot\nabla(ln\, n)) + \frac{\omega^2}{c^2}n^2\mathbf{E} = 0, \tag{3.14}$$

where $n = n' + in'' = \sqrt{1+\chi}$. For this inhomogeneous media, $n_0 = 1$ and $\delta n(\mathbf{r}) = n(\mathbf{r}) - n_0$, $k_0 = \omega n_0/c$, $\mathbf{r} = (\mathbf{r}_\perp, z)$, $\mathbf{E}(\mathbf{r},t) = \mathtt{exp}(ik_0z - i\omega t)\mathbf{A}(\mathbf{r}_\perp, z)$. We assume that the field has linear polarization set to y direction. And at the entrance, it is given by

$$\mathbf{A}(x,0) = A_0\mathtt{exp}[-(\frac{x-x_0}{w_0})^2]\hat{y}, \tag{3.15}$$

where $w_0 = 0.1mm$ is the beam waist. $x_0 = 0.1mm$ is the beam center at the entrance.

To get an accurate result we go beyond the paraxial limit following the method of [53, 54]. Separate the field into transverse and longitudinal components and expand the equation on the small parameters λ/w_0 and δn, we obtain

$$i\frac{\partial A_y}{\partial z} = \frac{1}{2n_0k_0}(\frac{\partial^2\delta n}{\partial x^2}A_y + 2\frac{\partial\delta n}{\partial x}\frac{\partial A_y}{\partial x} + \delta n\frac{\partial^2 A_y}{\partial x^2})$$

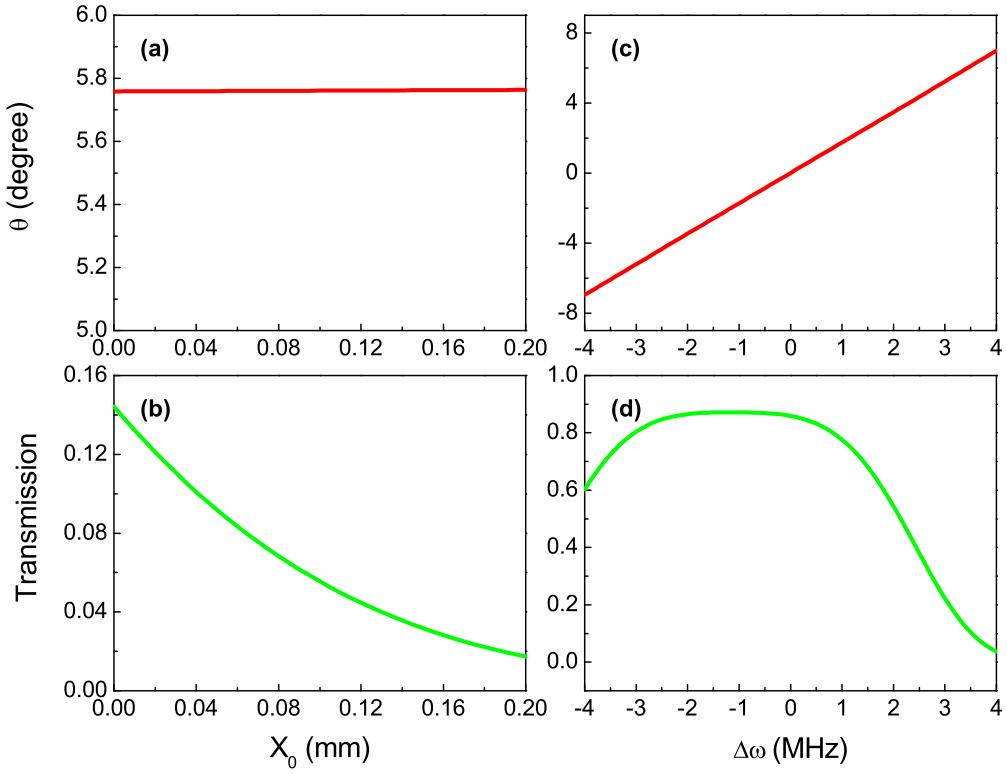

Fig. 10. Deflection angle and transmission curves for the profile $\Omega(x) = \Omega_0/\sqrt{1+\beta x}$. In (a,b) the detuning is fixed at $\Delta\omega = 3.3MHz$, the angle is constant when X_0 varying from 0 to $0.2mm$. In (c,d) $X_0 = 0$ while $\Delta\omega$ changes from $-4MHz$ to $4MHz$, the angle follows the detuning linearly.

$$-\frac{1}{2k_0}\frac{\partial^2 A_y}{\partial x^2} - \frac{k_0\delta n}{n_0}A_y. \tag{3.16}$$

It is then straightforward to get the beam profile at $z > 0$. To compare with the result in Fig. 10(a,b) we use the same parameters. The only difference is now it is a beam instead of a ray. Simulation result is shown in Fig. 11. It clearly exhibits the beam being deflected and absorbed as it propagates along the z axis. The peak of the beam goes to $X_1 = 0.556mm$. This is a little smaller than the value $X_1 = 0.600mm$ of a ray starting from $X_0 = 0.1mm$, which is reasonable since the absorption increases with

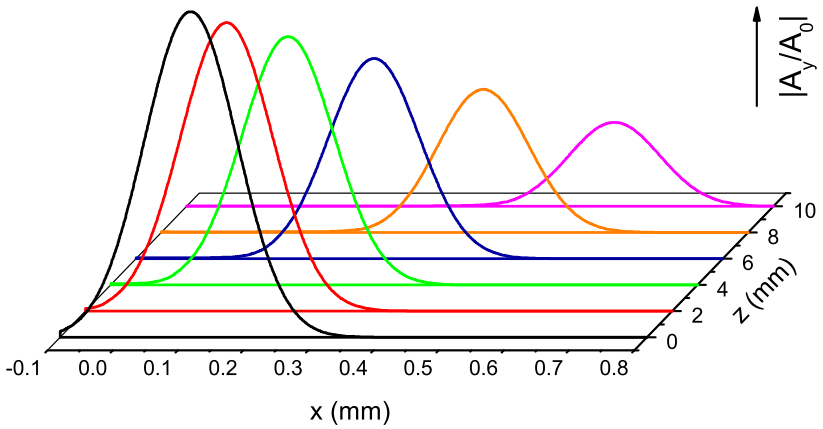

Fig. 11. Numerical simulation for beam propagation. Here detuning $\Delta\omega = 3.3MHz$.

x and thus lower the peak position. The peak intensity of the beam is $|A_y/A_0|^2 = 0.0664$, slightly higher than the ray transmission 0.0555. The deflection angle from the simulation is 5.75°, matching the former result precisely. This angle is almost a constant for the whole beam despite its extremely slow increasing with z.

From this example we see the deflection angle could be as large as

$$\theta \simeq 0.1rad, \tag{3.17}$$

with affordable losses, which shows a potential for an all-optical light steering. Here the deflection angle is only constant for a single frequency, but this is not a big problem for a probe pulse with narrow bandwidth.

As we have mentioned before, other drive field profiles will lead to spread of the probe pulse because the refractive index gradient depends on the spatial coordinates (see Fig. 9b). Consider the simplest case $\Omega(x) = \Omega_0(1 + \beta x)$, which gives $n'(x) = 1 + \alpha_0\Delta\omega/(1 + \beta x)^2$. $\beta = 1500/m$ and all the other parameters same as the first case. Now probe ray with $\Delta\omega = 3.3MHz$ starting from different X_0 have different deflection angles, as shown in Fig. 12. It spreads even for a single frequency, so is not

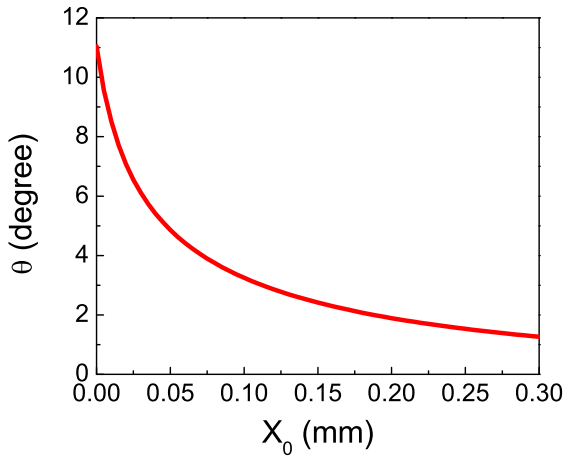

Fig. 12. Beam spreading for the profile $\Omega(x) = \Omega_0(1 + \beta x)$. The detuning is fixed at $\Delta\omega = 3.3MHz$. The deflection angle is not a constant for varying X_0.

suitable for beam steering.

2. Focusing and defocusing

Next we show that, by controlling the spatial dependence of the Rabi frequency of the drive field, we can have focusing or defocusing coherent media which adds additional flexibility to handle the probe field. Thus the coherent medium can not only act as an effective beam deflector but also it can be transformed into a lens with controllable focal distance. We recall that in both Moseley and Mitsunaga papers they are using Gaussian coupling beams so the focusing is not quite intense [47, 49]. Here we assume that the Rabi frequency of the drive field depends on the transverse coordinate via

$$\Omega(x) = \frac{\Omega_0}{\sqrt{1 - \beta x^2}}. \tag{3.18}$$

The space dependent refractive index is then given by $n'(x) = 1+\alpha_0\Delta\omega(1-\beta x^2)$. This creates the ray structure shown in Fig. 9c. To see this, we consider a ray that starts

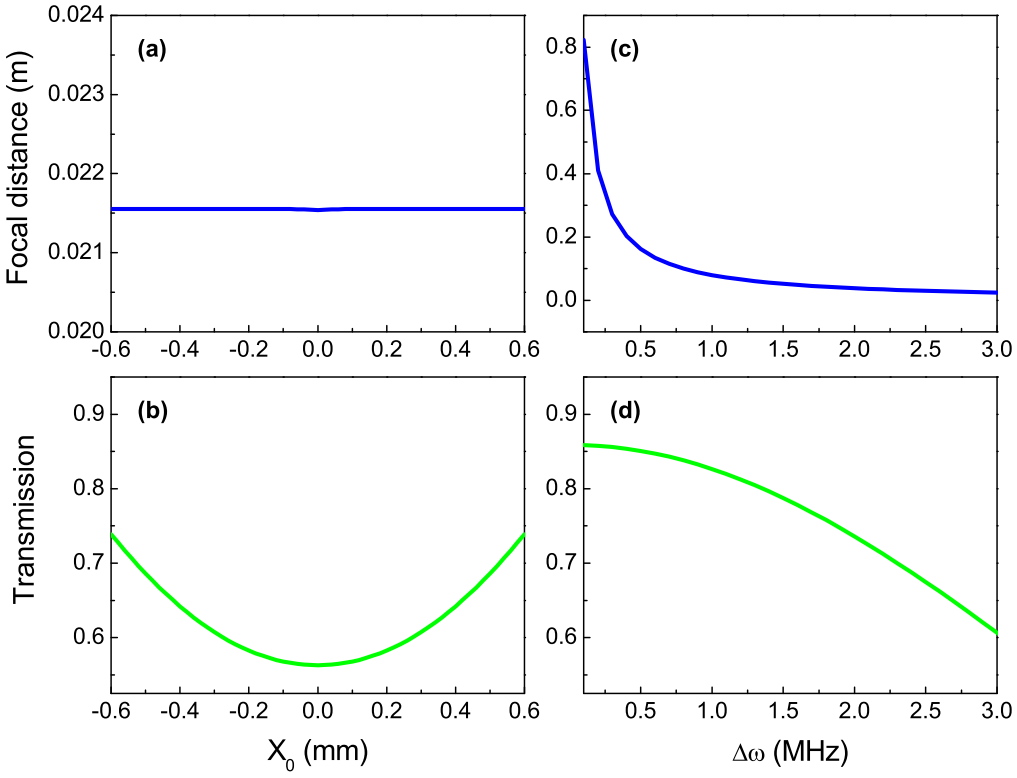

Fig. 13. Focusing effect for the profile $\Omega(x) = \Omega_0/\sqrt{1-\beta x^2}$. In (a,b) the detuning is fixed at $\Delta\omega = 3.3MHz$, the focal distance is constant when X_0 varying from $-0.6mm$ to $0.6mm$. In (c,d) $X_0 = 0$ while $\Delta\omega$ changes from $0.1MHz$ to $3MHz$, the angle follows (3.19).

at X_0. As a simple estimate, it goes out of the cell at $X_1 = X(L) \simeq X_0(1-\alpha_0\Delta\omega\beta L^2)$ and the deflection angle is $\theta \simeq -2\alpha_0\Delta\omega\beta L X_0$. This ray passes the axis at the distance

$$F = \frac{X_1}{-\theta} \simeq \frac{1-\alpha_0\Delta\omega\beta L^2}{2\alpha_0\Delta\omega\beta L}, \tag{3.19}$$

which is independent of the initial position of the ray, X_0. This represents a lens with a focal distance F.

The calculation based on full expression also supports these estimates. Consider a system with $\Delta\omega = 3.3MHz, \beta = 10^6/m^2$ and all the other parameters same to the

first case. It is obvious from Fig. 13a that F does not change after X_0. So the focal distance F is well defined for a single frequency. However, this distance changes for different frequencies (see Fig. 13c) as in (3.19). It decreases for large detuning which is easy to understand since large detuning has rapid refractive index change and the beam deflects quickly. The focal distance F can also be controlled by varying Ω_0 or β. Both smaller Ω_0 and larger β can lead to smaller focal distance. The reason is the same as above. Finally, using a negative β or negative $\Delta\omega$ we can obtain good defocusing effect. If both β and $\Delta\omega$ are negative we get focusing again. This is more applicable for experiment since the highest drive field required is Ω_0 at the center. Note here the drive field depends on x so this is only a 2D focusing. To simulate a real lens it should depend on $r_\perp$.

3. Short pulse deflection

Up to now our discussion applies to the propagation of continuous waves and pulses that have time duration long enough to fit the EIT window, i.e. $\Omega^2 T/\gamma > 1$, where T is the pulse width. The problem with shorter pulses is that they have a broad spectrum that may not fit the EIT window, leading to substantial absorption and a nonlinear dispersion. As a result, we may encounter strong reshaping and absorption while the pulse propagates through the EIT medium.

In last chapter, we proposed a solution to the problem of broadband pulse propagation through the EIT medium [55]. We mentioned that the EIT medium provides a deflection effect in that scheme. The gradient of the refractive index comes from the gradient of the magnetic field, because the detuning is position dependent. Simply remove the phase shifter and we have a scheme for short pulse deflection. The scheme is depicted in Fig. 14. The system consists of a set of prisms (or diffraction gratings) with total dispersion equal to zero. The first prism disperses the probe pulse into a

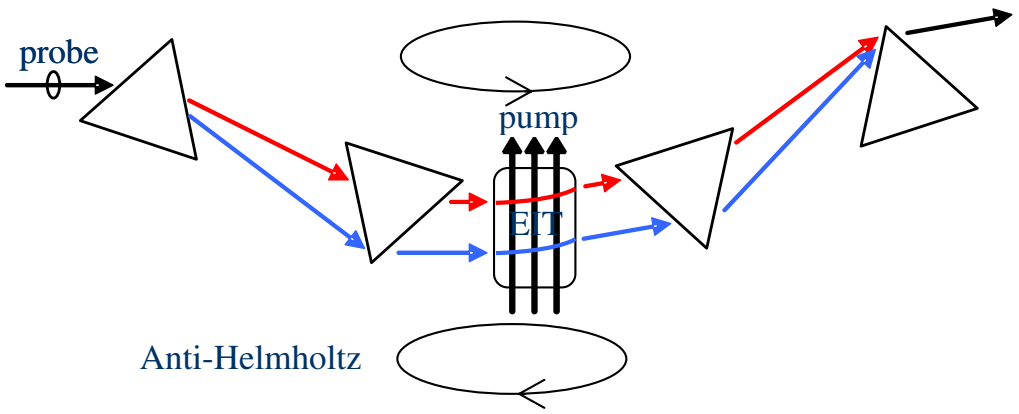

Fig. 14. Scheme for broadband pulse deflection.

divergent beam. The second prism transforms the beam into a parallel beam, with different frequencies shifted in space. When the beam goes into the EIT cell with cold atoms, an inhomogeneous magnetic field moves the level b only so that each frequency is resonant with the local $a \leftrightarrow b$ transition. At the same time, the constant drive field propagates along the x direction, which is resonant with $a \leftrightarrow c$ transition.

Now a single frequency ray at different x positions will see different detunings and refractive indexes because ω_{ab} changes with x due to the applied inhomogeneous magnetic field. Such a refractive index gradient will cause deflection. For an ideal system, the frequency distribution after the second prism is linear, i.e., $d\omega/dx$ is a constant. Also $d\omega_{ab}/dx$ should be the same to match the field. We assume that a ray of frequency ω enters the EIT cell at x_0 position, and define $\delta x = x - x_c$ where x_c is the position the ray is resonant, i.e, $\omega = \omega_{ab}(x_c)$. So the detuning at position x is

$$\Delta\omega(\delta x) = \omega - \omega_{ab}(x) = \omega_{ab}(x_c) - \omega_{ab}(x) = -\delta x \frac{d\omega_{ab}}{dx}. \tag{3.20}$$

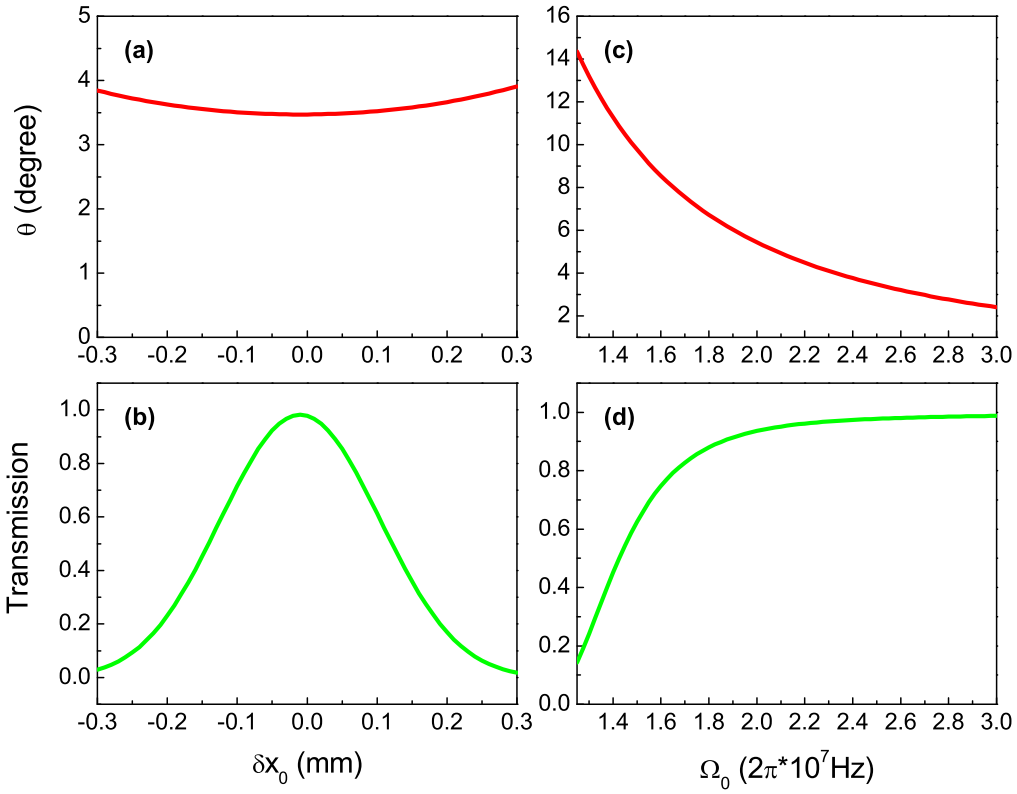

Fig. 15. Deflection angle and transmission for the broadband pulse. Their dependence on the position of the probe ray, δx_0 (a,b) and on the magnitude of the Rabi frequency (c,d).

The refractive index will be

$$n'_\omega(\delta x) \simeq 1 + \alpha_0 \Delta\omega(\delta x) = 1 - \alpha_0 \delta x \frac{d\omega}{dx}. \tag{3.21}$$

The refractive gradient $\nabla n' = -\alpha_0 (d\omega/dx)\hat{x}$ is a constant. It follows from (3.12)(3.13) that $\delta x_1 - \delta x_0 \simeq |\nabla n'| L^2/2$ and $\sin\theta \simeq |\nabla n'| L$ for small deflection. They do not depend on δx_0 or ω. So all the rays go through parallel paths. This is crucial for the recombination of the pulse. Thus a probe beam with finite bandwidth and finite diameter can be deflected perfectly.

The above is only a simple estimate. In Fig. 15 we show some numerical results for $d\omega/dx = -10^{11}Hz/m, L = 1mm$ and all the other parameters same to the first case. In Fig. 15a and 15b we can see the rays of frequency $2\pi \times 6 \times 10^{14}Hz$ starting from different δx_0, the deflection angles are around 3.47° although a little larger for nonzero δx_0. The transmission for $\delta x_0 = 0$ is the highest (0.98) but decreases quickly for other starting positions. This is good enough since we can always put the central rays, which are the main part for an ordinary beam, at $\delta x_0 = 0$. Unlike the first case now the frequency does not influence the deflection angle. Calculation for ω varying by $10^{10}Hz$ still gives the same curve, which is reasonable because only local decays are slightly changed. As a result the whole beam, despite its diameter and bandwidth, deflects in the same angle. If the diameter is small enough to fit within $\delta x_0 = \pm 0.05mm$, the whole pulse will be deflected with transmission ~ 1.

We can control the angle by varying the drive Rabi frequency, as shown in Fig. 15(c,d). The parameters are still the same, $\lambda = 5000\mathring{A}$, $\delta x_0 = 0$, only Ω varying from $2\pi \times 1.25 \times 10^7 Hz$ to $2\pi \times 3 \times 10^7 Hz$. It is easy to find from the graph that the larger deflection angle accompanies smaller transmission. Even angle greater than 10° is achievable at small drive field. But then the side rays (nonzero δx_0) suffer substantial absorption. For large drive field the system goes to the limit angle $\theta \to 0$ and transmission $\to 1$.

D. Conclusion

We have shown that for single frequency or narrow bandwidth probe field, high quality deflection and focusing can be achieved under optimal profiles. The practical difficulty is how to generate such profiles. One possible way is to put a screen with the desired transmission function as in (3.9)(3.18) behind the drive field. The drive

field diffraction may not be so severe if the propagation distance is short. Then we can control the deflection angle or focal distance by only varying the input drive field intensity ($\propto \Omega_0$). This method is convenient and continuous. However, the scan speed is limited by the EIT establishment time, which is about the radiative lifetime $1/\gamma_{rad}$.

A short pulse can also be deflected to the same angle in the proposed scheme. The key point is here the magnetic gradient provides the same refractive index gradient for all the frequency components. The deflection angle can also be controlled by the drive intensity. This method is promising due to its broadband ability. Here the problem is the lowest frequency gradient of a real prism system is $10^{14} Hz/m$ and it is only approximately constant. We need a better system to provide larger spatial dispersion.

In both of the deflection schemes the maximum deflection angle without significant absorption is $\sim 0.1 rad$. Larger deflection always comes with larger absorption. This is determined by the relation between refractive index and absorption coefficient in EIT. Note $0.1 rad$ is already good enough for some applications. And additional devices like multiple birefringent prisms or holographic glass with multiple holograms can further increase the angle.

CHAPTER IV

ELECTROMAGNETICALLY INDUCED TRANSPARENCY INSIDE THE LASER CAVITY: SWITCH BETWEEN FIRST-ORDER AND SECOND-ORDER PHASE TRANSITIONS*

A. Introduction

Lasing is a cooperative phenomenon of many atoms in the cavity. Each atom has a dipole induced by the field from all the other atoms, in turn its dipole also contributes to the field, which can be uniformly treated by the mean field theory. Although laser is a non-equilibrium system, the formal similarity enables the analogy of its near-threshold behavior to second-order phase transitions in the equilibrium systems [56, 57, 58]. For example, in the analogy to the ferromagnetic phase transition, the electric field corresponds to the magnetization M, the unsaturated population inversion corresponds to the temperature, and an injected field corresponds to the external magnetic field H. The measurement of the laser "coexistence curve" and "susceptibility" below threshold confirmed this analogy quantitatively [59]. As a completion of this analogy, Gatti and Lugiato showed that the correlation length of a degenerate optical parametric oscillator diverges when it approaches the threshold [60].

Once the second order phase transition analogy was established, people started looking for similar analogy in first-order. Examples include the laser with a saturable

---

*Reprinted with permission from "Electromagnetically induced transparency inside the laser cavity: Switch between first-order and second-order phase transitions" by Q. Sun, M. Selim Shahriar and M. S. Zubairy, 2008. *Phys. Rev. A*, vol. 78, pp. 013805, Copyright [2008] by the American Physical Society.

absorber (LSA) [61, 62, 63, 64, 65], and the dye laser [66, 67]. Here we will concentrate on the LSA problem. The saturable absorber is inside the laser cavity. The absorption saturation changes the nature of the system. So the laser output can have two stable values and leads to bistability, hysteresis, etc. Experiments have been done in many systems, e.g., $He : Ne$ laser [68, 69], CO_2 laser with SF_6 absorber [70], and N_2O laser with NH_3 absorber [71]. In theory, Mandel and coworkers treated the problem analytically in both semiclassical and quantum theories [72]. In their model both the active cell and the absorber cell contain two-level atoms, interacting with a single cavity mode. The relative saturability and population inversion of the two cells determine the number of roots. Hysteresis cycle is obtained when two stable roots are available. The quantum theory based on Fokker-Planck equation gives the field fluctuation and linewidth across the threshold. It is shown that the finite fluctuation increase drastically when approaching the threshold, and then goes to zero above the threshold. The linewidth also has a sharp narrowing. In a related paper [73] they showed the including of higher order derivative terms reduces the width of the transition region, making the transition threshold much sharper. This model has also been used to study the time-dependent behavior [74, 75]. Small amplitude harmonically modulated intensity and the pulsed solution corresponding to the passive Q switching are found to be the stable solutions. Roy gave the photon distribution in this system and showed the similarity to the dye laser [76].

As another concept in the phase transition theory, a tricritical point is the joint of a line of the first-order phase transition to a second-order line in the parameter space. Scott pointed out the existence of tricritical point in his LSA model [77]. Mortazavi and Singh measured the tricritical behavior by changing the discharge current of the absorber cell [78]. Later they found that the intensity fluctuation undergoes a qualitative change through the tricritical point [79]. For a second-order phase

transition, the fluctuation decreases from the thermal value to zero with increasing excitation, while for a first-order phase transition it first increases to a superthermal value and then decreases to zero.

Systems that have multistability and multicritical points are also explored [80, 81, 82]. It is shown that when the potential has higher order terms or when multimode laser introduces more order parameters, there could be multistability and multicritical points.

Three-level systems have also been used to model the absorber. One example is the two-photon absorber [83], in which the middle level is assumed to be far from resonance so that the system is very similar to a two-level system. Agrawal considered the case of a Λ system [84]. The laser frequency is assumed to lie midway between the ground state sublevels. The phase transition is determined by the detuning, which can be controlled by a static electric or magnetic field. He predicted the switch between first-order and second-order phase transitions similar to our result, although the mechanism is different.

The system we proposed is also based on EIT. The laser field resonant with one transition should have been absorbed. But at the presence of another drive field resonant with another transition with a common level, the coherence effect renders transparency for the laser field. This property intrigues our interest in the possible application into LSA problem. Since the drive field can control the absorption of the probe field, it might simulate a system of laser with or without saturable absorber. As a result, we would be able to switch between first-order and second-order phase transitions by simply adjusting the drive field intensity.

B. Free energy for a laser with/without a saturable absorber

From Landau's theory the Gibbs free energy close to a critical point can be expanded into even powers of a displacement parameter x,

$$G(x) = C_2 x^2 + C_4 x^4 + C_6 x^6 + \ldots, \tag{4.1}$$

where the coefficient C_2 is linear to the difference between the reservoir variable and its critical value. The phase transition is second-order if C_4 is positive, while first-order if C_4 is negative.

A potential similar to the Gibbs free energy can be defined for a laser [56]. The displacement parameter is the electric field $\mathscr{E}$. One can obtain a Fokker-Planck equation from the laser theory and then apply it to the electric field to get a equation of motion for the expectation value. The potential can then be obtained by integration from

$$\dot{\mathscr{E}} = -\frac{\partial G(\mathscr{E})}{\partial \mathscr{E}}. \tag{4.2}$$

For a laser without absorber, the equation of motion is well known as

$$\dot{\mathscr{E}} = \frac{1}{2}\left[(\mathscr{A} - \mathscr{C})\mathscr{E} - \mathscr{B}\mathscr{E}^3\right], \tag{4.3}$$

here $\mathscr{A}$ is the unsaturated gain in the active medium, $\mathscr{B}$ is the saturation parameter, and $\mathscr{C}$ is the cavity loss. Both $\mathscr{A}$ and $\mathscr{B}$ are proportional to the population inversion σ. A simple integration gives $C_4 = \mathscr{B}/8$ which is positive. So it is a second-order phase transition. The stable value of $\mathscr{E}$ changes continuously as one move across the critical point.

For a laser with a saturable absorber inside the cavity, the equation of motion

can be modified as [65]

$$\dot{\mathscr{E}} = \frac{1}{2}\left[(\mathscr{A} - \mathscr{C} - \frac{S}{1+\mathscr{E}^2/I_s})\mathscr{E} - \mathscr{B}\mathscr{E}^3\right], \tag{4.4}$$

where S is the linear absorption from the saturable absorber and I_s is the saturation intensity. After integration the potential has a logarithmic term coming from the saturable absorber. Power series expansion gives

$$C_4 = \frac{1}{8}(\mathscr{B} - \frac{S}{I_s}). \tag{4.5}$$

So if the saturation intensity of the absorber is small $I_s \leq S/\mathscr{B}$, the phase transition would be first-order. The field has a discontinuous jump from zero to some finite value when crossing the critical point.

C. Derivation and discussion

The setup for our system is shown in Fig. 16. We use a unidirectional ring laser cavity and assume both kinds of atoms are homogenously broadened. The incoherent pumping in the gain medium provides population inversion for the active atoms, generating a laser field as the probe field for the Λ-type three-level atoms in the absorber cell. This probe field with frequency ν interacts with the transition $|a\rangle \leftrightarrow |b\rangle$. While the external drive field with frequency ν_μ interacts with the transition $|a\rangle \leftrightarrow |c\rangle$. To avoid drive field recycling we assume the mirrors to be transparent to the drive field.

For a closed system, the density matrix equations are

$$\dot{\rho}_{bb} = \Gamma_{ab}\rho_{aa} + \Gamma_{cb}\rho_{cc} - \frac{i}{2\hbar}\left(\wp_{ab}\mathscr{E}e^{-i\nu t}\rho_{ba} - c.c.\right), \tag{4.6}$$

$$\dot{\rho}_{cc} = \Gamma_{ac}\rho_{aa} - \Gamma_{cb}\rho_{cc} - \frac{i}{2}\left(\Omega_\mu e^{-i\phi_\mu}e^{-i\nu_\mu t}\rho_{ca} - c.c.\right), \tag{4.7}$$

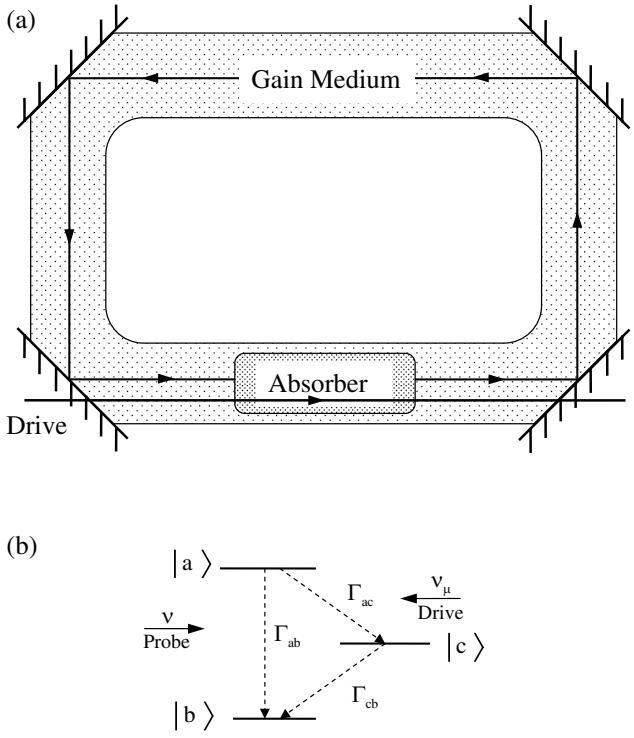

Fig. 16. The setup of EIT in a laser cavity. (a) The absorber cell filled with three-level atoms is put inside the unidirectional ring laser cavity. (b) The level structure for the three-level atoms.

$$\dot{\rho}_{aa} = -(\Gamma_{ab} + \Gamma_{ac})\rho_{aa} + \frac{i}{2\hbar}\left(\wp_{ab}\mathscr{E}e^{-i\nu t}\rho_{ba} - c.c.\right) + \frac{i}{2}\left(\Omega_\mu e^{-i\phi_\mu}e^{-i\nu_\mu t}\rho_{ca} - c.c.\right), \quad (4.8)$$

$$\dot{\rho}_{ab} = -(i\omega_{ab} + \gamma_{ab})\rho_{ab} - \frac{i\wp_{ab}\mathscr{E}}{2\hbar}e^{-i\nu t}(\rho_{aa} - \rho_{bb}) + \frac{i}{2}\Omega_\mu e^{-i\phi_\mu}e^{-i\nu_\mu t}\rho_{cb}, \quad (4.9)$$

$$\dot{\rho}_{cb} = -(i\omega_{cb} + \gamma_{cb})\rho_{cb} - \frac{i\wp_{ab}\mathscr{E}}{2\hbar}e^{-i\nu t}\rho_{ca} + \frac{i}{2}\Omega_\mu e^{i\phi_\mu}e^{i\nu_\mu t}\rho_{ab}, \quad (4.10)$$

$$\dot{\rho}_{ca} = -(i\omega_{ca} + \gamma_{ca})\rho_{ca} + \frac{i}{2}\Omega_\mu e^{i\phi_\mu}e^{i\nu_\mu t}(\rho_{aa} - \rho_{cc}) - \frac{i\wp_{ba}\mathscr{E}^*}{2\hbar}e^{i\nu t}\rho_{cb}, \quad (4.11)$$

where $\wp_{ab}$ is the the electric dipole moment, $\mathscr{E}$ is the probe field produced by the active atoms, Ω_μ is the drive Rabi frequency, Γ and γ are the population relaxation

rates and dipole dephasing rates, respectively.

For simplicity, we assume both the drive field and the probe field to be resonant with their corresponding transitions. After transforming into the rotating frame,

$$\rho_{ab} = \widetilde{\rho}_{ab} e^{-i\omega_{ab}t}, \rho_{cb} = \widetilde{\rho}_{cb} e^{-i(\omega_{ab}-\nu_\mu)t}, \rho_{ca} = \widetilde{\rho}_{ca} e^{i\nu_\mu t}. \tag{4.12}$$

Together with the relation $\rho_{aa} + \rho_{bb} + \rho_{cc} = 1$ for the closed system, we can obtain the steady state solution. So the effective polarization from the absorber

$$\begin{aligned}\mathscr{P} = 2N_a^e \wp_{ba}\widetilde{\rho}_{ab} = iN_a^e \frac{|\wp_{ab}|^2 \mathscr{E}}{\hbar D}\Bigg\{\left|\frac{\wp_{ab}\mathscr{E}}{2\hbar}\right|^2 (\Gamma_{ab}+\Gamma_{ac})\Gamma_{cb} \\ +\gamma_{cb}\left[\frac{\Omega_\mu^2}{2}(\Gamma_{ab}+\Gamma_{cb}) + \gamma_{ca}(\Gamma_{ab}+\Gamma_{ac})\Gamma_{cb}\right]\Bigg\},\end{aligned} \tag{4.13}$$

where the denominator

$$\begin{aligned}D = \left|\frac{\wp_{ab}\mathscr{E}}{2\hbar}\right|^4 (2\Gamma_{ac}+4\Gamma_{cb}) + \left|\frac{\wp_{ab}\mathscr{E}}{2\hbar}\right|^2 [\gamma_{ab}(\Gamma_{ab}+\Gamma_{ac})\Gamma_{cb} + \\ +\frac{\Omega_\mu^2}{2}(\Gamma_{ab}+\Gamma_{ac}-3\Gamma_{cb}+6\gamma_{cb}) + 2\gamma_{cb}\gamma_{ca}(\Gamma_{ac}+2\Gamma_{cb})\Bigg] \\ +(\frac{\Omega_\mu^2}{4}+\gamma_{ab}\gamma_{cb})\left[\frac{\Omega_\mu^2}{2}(\Gamma_{ab}+\Gamma_{cb}) + \gamma_{ca}(\Gamma_{ab}+\Gamma_{ac})\Gamma_{cb}\right],\end{aligned} \tag{4.14}$$

and N_a^e is the effective number density for the three-level atoms. It can be related to the actual number density by $N_a^e = N_a V_a / V_{tot}$. Here V_a and V_{tot} are the absorber volume and the total volume, respectively. Similarly we can define the effective number density for the gain medium N_g^e.

We assume the active system to be homogeneously broadened two-level system, which has the same level separation as ω_{ab} and the same dipole moment. The field equation of motion is

$$\dot{\mathscr{E}} = \frac{1}{2}\left[(\frac{\mathscr{A}}{1+\mathscr{E}^2/I_s} - \mathscr{C})\mathscr{E} - (\frac{\nu}{\epsilon_0})Im\mathscr{P}\right], \tag{4.15}$$

here $\mathscr{A} = \frac{\nu|\wp_{ab}|^2 N_g^e}{\epsilon_0 \hbar \gamma_{ab}}$ and $I_s = \frac{\hbar^2 \Gamma_{ab}^2}{2|\wp_{ab}|^2}$ is the saturation intensity for the active atoms. After integration the coefficient of $\mathscr{E}^4$ term in $G(\mathscr{E})$ is

$$\begin{aligned} C_4 &= \frac{1}{8}\frac{\mathscr{A}}{I_s} - \frac{\nu}{2} N_a^e \frac{|\wp_{ab}|^4}{4\epsilon_0 \hbar^3} \times \\ &\times \frac{\frac{\Omega_\mu^2}{4}\left[2\gamma_{cb}(\Gamma_{ab}+\Gamma_{ac}-3\Gamma_{cb}) - (\Gamma_{ab}+\Gamma_{ac})\Gamma_{cb} + 12\gamma_{cb}^2\right] + 2\gamma_{cb}^2\gamma_{ca}(\Gamma_{ac}+2\Gamma_{cb})}{4(\frac{\Omega_\mu^2}{4}+\gamma_{ab}\gamma_{cb})^2\left[\frac{\Omega_\mu^2}{2}(\Gamma_{ab}+\Gamma_{cb}) + \gamma_{ca}(\Gamma_{ab}+\Gamma_{ac})\Gamma_{cb}\right]}. \end{aligned} \tag{4.16}$$

If there is no drive field, i.e., $\Omega_\mu = 0$, it is simplified

$$C_{4(\Omega_\mu=0)} = \frac{1}{8}\frac{\mathscr{A}}{I_s} - \frac{\nu}{2} N_a^e \frac{|\wp_{ab}|^4}{4\epsilon_0 \hbar^3} \frac{\Gamma_{ac}+2\Gamma_{cb}}{2\gamma_{ab}^2(\Gamma_{ab}+\Gamma_{ac})\Gamma_{cb}}. \tag{4.17}$$

For large enough N_a^e we could have $C_{4(\Omega_\mu=0)} < 0$. Then we increase the drive field intensity so that the second term of (4.17) has a smaller magnitude. Finally at some point $C_4 = 0$. According to Ref [65] this is the criterion between first-order and second-order phase transitions.

In the limiting case of a perfect EIT system, the dephasing rate between the two lower levels $\gamma_{cb} = 0$, which also requires $\Gamma_{cb} = 0$. Substitute into the (4.17,4.17) we find $C_{4(\Omega_\mu \neq 0)} = \mathscr{A}/8I_s$ while $C_{4(\Omega_\mu=0)} \to -\infty$. One might say that the phase transition is second-order or first-order, just depends on whether we switch on the drive field or not. But the stable value of $\mathscr{E}$ would also goes to infinity so it is a idealized situation. One can never achieve a perfect EIT.

For a finite γ_{cb} we did the numerical calculation to find the steady state solutions for (4.15). These solutions will follow the change of $\mathscr{C} = \nu/Q$ where Q is the quality factor of the cavity. As can be seen from Fig. 17, the probe intensity-Q curve is single valued for a Rabi frequency above the threshold, while bistable for a Rabi frequency below the threshold. Those parts with a negative slope are unstable. So the switch between first-order and second-order phase transitions can be achieved by simply changing the drive Rabi frequency. For a small range near the threshold there are

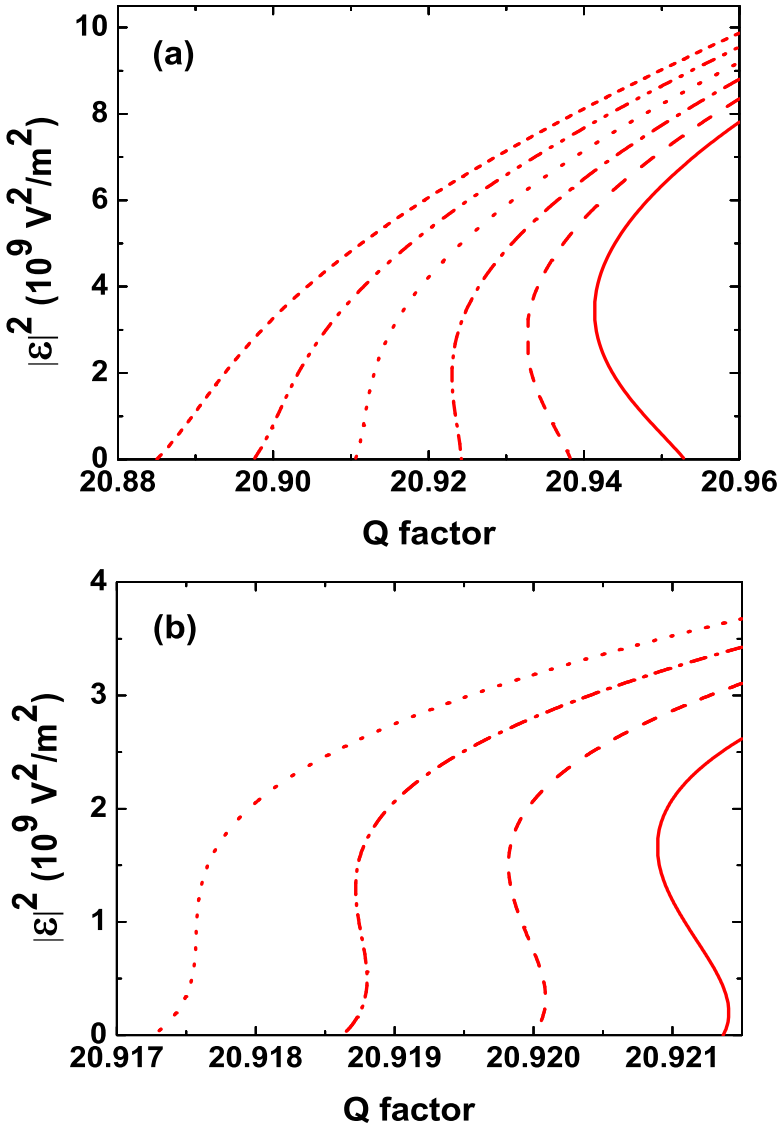

Fig. 17. Intensity-Q factor curves for different drive Rabi frequencies. (a) From right to left, $\Omega_\mu = 0.100MHz$, $0.104MHz$, $0.108MHz$, $0.112MHz$, $0.116MHz$, $0.120MHz$. Clearly there is a switch between first-order and second-order phase transitions. (b) From right to left, $\Omega_\mu = 0.1088MHz$, $0.1092MHz$, $0.1096MHz$, $0.1100MHz$. For a small range near tricritical point, there could be three nonzero solutions. The other parameters are $|\wp_{ab}| = 10^{-29}m \cdot C$, $\lambda = 1\mu m$, $N_a^e = 4.5 \cdot 10^{16}m^{-3}$, $N_g^e = 1.28 \cdot 10^{18}m^{-3}$, and $\gamma_{cb} = 1kHz$.

even three solutions. When the Q factor increases, one can see a second-order phase transition followed by a first-order phase transition, as shown for $\Omega_\mu = 0.1096 MHz$.

The parameters we used are somehow extreme. The Q factor and drive Rabi frequency are small. But the probe laser intensity is large, which is still acceptable since it is inside the cavity. There is no requirement for a small probe because we keep $\mathscr{E}$ to all order in (4.13). An interesting thing is to compare the threshold value to the solution of $C_4 = 0$. Ideally they should be the same. But we found a small difference. This can be understood since the C_4 expression is obtained from small probe approximation, which does not apply quite well in this case.

The switch between first-order and second-order phase transition is a tricritical point in the phase space, as can be seen from the phase diagram Fig. 18. Such tricritical points have been predicted in the two-level atom saturable absorber case [78]. In that system the point is the termination of both lines, while here the first-order line goes beyond the tricritical point. So for a given drive Rabi frequency, we can observe a first-order transition, or a second-order transition followed by a first-order transition, or a second-order transition.

We use the Q factor as the variable to investigate the phase transition because it is the only parameter not in the expression of C_4. So we can compare the criterion $C_4 = 0$ to the numerical results. Without that purpose other parameters may also be used as the variable, for example, the effective number density of the gain medium. It is proportional to the discharge current if we use a gas discharge cell as the gain cell [78]. The numerical calculation shown in Fig. 19 is similar to Fig. 17. For a given drive Rabi frequency there could be one, two, or three solutions.

The latent heat in first-order phase transition is also an interesting topic [65]. At

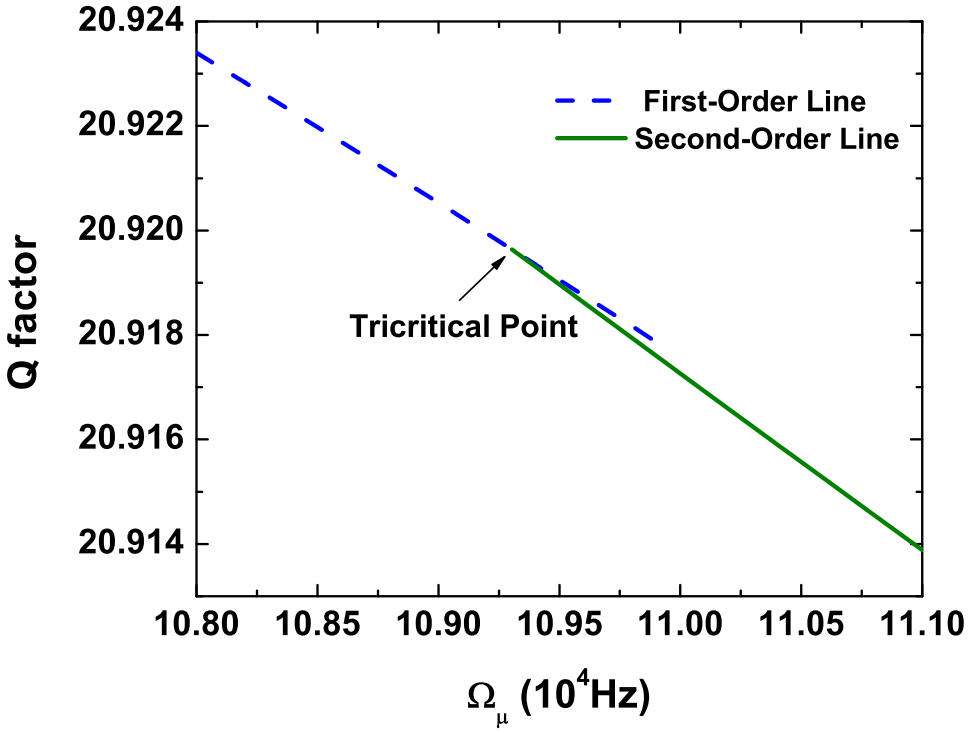

Fig. 18. Phase diagram for the system. The first-order phase transition line meets the second-order line at the tricritical point and goes beyond.

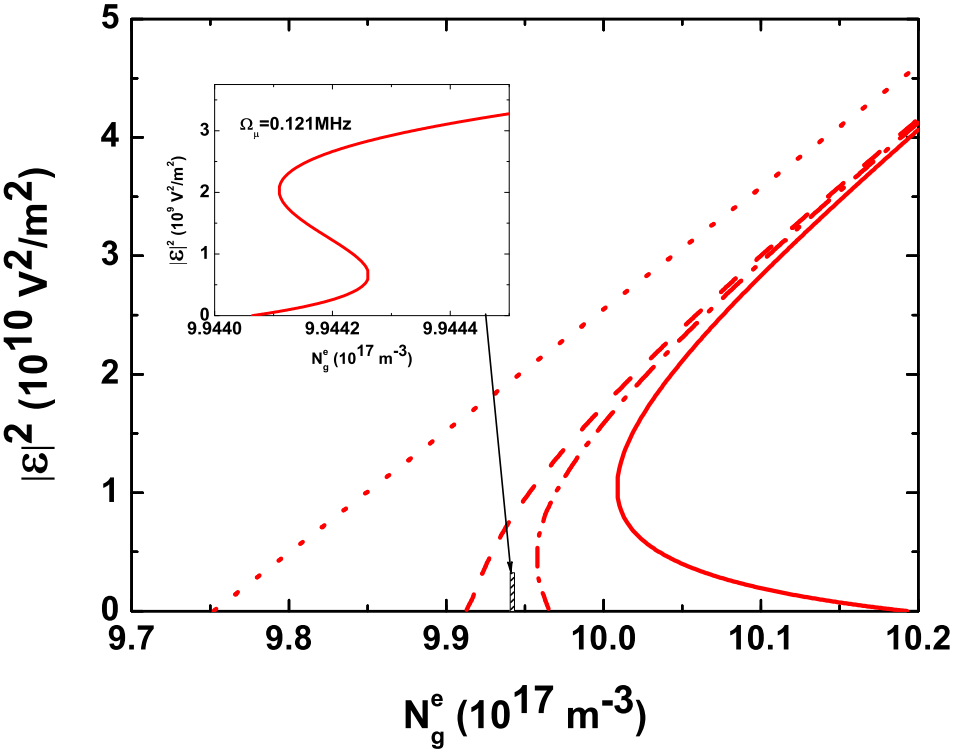

Fig. 19. Intensity-N_g^e curves for different drive Rabi frequencies. From right to left, $\Omega_\mu = 0.011MHz$, $0.11MHz$, $0.14MHz$, $1.1MHz$. Similarly there is a switch between first-order and second-order phase transitions. In the small window enlarged around the tricritical point, $\Omega_\mu = 0.121MHz$ and there are three nonzero solutions. The other parameters are $|\wp_{ab}| = 10^{-29}m \cdot C$, $\lambda = 1\mu m$, $N_a^e = 4.5 \cdot 10^{16}m^{-3}$, $Q = 27$, and $\gamma_{cb} = 1kHz$.

the critical point, the Clausius-Clapeyron equation is

$$L = T_0(V_2 - V_1)\frac{dP}{dT_0}. \tag{4.18}$$

In our system, minus threshold population inversion corresponds to the critical temperature T_0, drive field corresponds to the pressure P, and the laser field corresponds to the volume V. $\mathscr{E}_1$ and $\mathscr{E}_2$ can be solved from (4.15).

LSA problem has also been investigated from the dispersive point of view. Mandel showed that if both cells contains two-level atoms, there could be new solutions corresponding to nonzero detuning because of the anomalous dispersion [85]. Lukin et al. considered the intracavity EIT and found a pronounced frequency pulling and cavity-linewidth narrowing [86]. Here we are mainly interested in the absorption property, so we take the detuning to be zero to avoid the pulling effect.

D. Conclusion

In this chapter, we investigate the effect of including an EIT cell as an absorber inside the laser cavity. By controlling the drive Rabi frequency, we can simulate the cases of laser with or without absorber and obtain phase transitions of both first-order and second-order. Around the tricritical point there could even be a second-order phase transition followed by a first-order one. These phenomena can be seen clearly from the phase diagram, in which the first-order phase transition line goes beyond its joint with the second-order line. The tricritical value determined by the criterion $C_4 = 0$ is close to the numerical result but not very accurate, because in this case the probe field is no longer small. Our calculation is based on Λ-type system. Other three-level systems like V-type or Ξ-type should have similar drive intensity controlled phase transition as well.

CHAPTER V

EFFECTS OF NOISE AND PARAMETER DEVIATION IN A BICHROMATIC RAMAN TYPE WHITE LIGHT CAVITY*

A. Introduction

In a Fabry-Perot cavity the round-trip phase delay is proportional to the frequency. Thus only certain discrete frequencies can be exactly resonant. If the cavity is filled with a medium which provides a negative dispersion and cancels the frequency dependence of the phase delay, a continuous range of spectrum can be resonant at the same time. Such a cavity is named as white light cavity (WLC) [87]. For precision measurements such as gravitational wave detection [88, 89, 90] and ring laser gyroscopes [91], the high sensitivity requires a high finesse Fabry-Perot cavity, at the price of a reduced bandwidth. WLC provides an effective way to increase the bandwidth and solves this dilemma.

The dispersion requirement for the medium is $\partial_\nu n = -1/\nu$, where the refractive index n is a function of the frequency ν. This is the so called λ-compensation or white light condition. A lot of systems are able to provide negative dispersion with small absorption or even gain [92, 93]. For example, for two-level atoms driven by a strong resonant field [94, 95], the probe dispersion is negative around the resonance. A variation of this scheme is the degenerate two-level system [96], in which there are two degenerate ground levels. Both the resonant drive field and the probe field

*Reprinted with permission from "Effects of noise and parameter deviations in a bichromatic Raman white light cavity" by Q. Sun, M. Selim Shahriar and M. S. Zubairy, 2010. *Phys. Rev. A*, vol. 81, pp. 033826, Copyright [2010] by the American Physical Society.

interact with the two transitions simultaneously. The advantage of this scheme is that it does not require a very strong drive field. For a Λ system with a bichromatic drive field far from resonance [97, 98], the probe field experiences a gain-doublet and the dispersion is negative at the center. Another system is double-Λ system in which the drive field interacts with the transitions from both ground levels to one of the excite level, and the probe field interacts with the transitions from both ground levels to the other excite level [88]. If instead using two drive fields in the double-Λ system, the propagation dynamics becomes important and it further enhances the cavity bandwidth [99]. Recently Savchenkov and co-workers demonstrated white light whispering gallery mode resonators [100]. For a resonator thick enough the modal spectrum becomes essentially continuous and the high quality factor is frequency-independent.

The idea of the gain-doublet scheme is proposed by Steinberg and Chiao during their pursuit of superluminal phenomena [101]. Wang et al. first realized it experimentally in a Λ system [97, 98]. Due to the negative dispersion, the group velocity can be superluminal or even negative. The ideal case of infinite group velocity is equivalent to the white light condition. The ability of this system to achieve the white light condition has been investigated by measuring the dispersion using a heterodyne technique [102], and by measuring the transmission spectrum [103]. A broadband cavity response has been observed.

In order to satisfy the white light condition we need to choose the parameters carefully. However, there are always deviations from the ideal values [88] and statistical noise. In this chapter we discuss the effects of parameter deviations and laser phase and amplitude noises in the bichromatic Raman system.

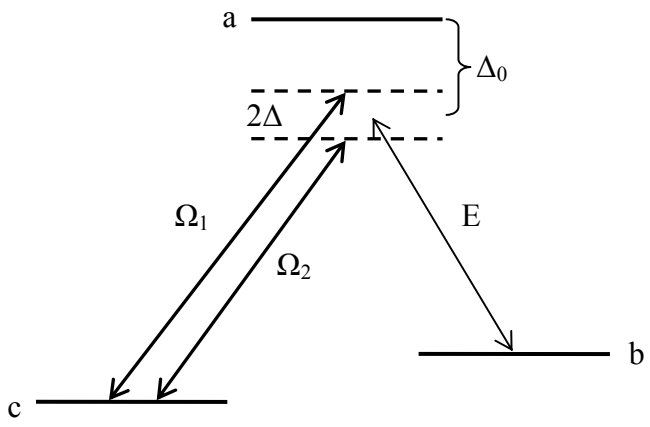

Fig. 20. The scheme of the bichromatic Raman system. The pump fields are far detuned from the single photon transition $|a\rangle \leftrightarrow |c\rangle$ and provides a gain-doublet for the probe field.

B. Parameter dependence of the susceptibility

The level structure of the bichromatic Raman system is shown in Fig. 20. There are two drive fields with frequencies ν_1 and ν_2 and Rabi frequencies Ω_1 and Ω_2, respectively. They are far detuned from the transition $|a\rangle \leftrightarrow |c\rangle$ with the detunings $\Delta_0+\Delta$ and $\Delta_0-\Delta$, where $\Delta = (\nu_1-\nu_2)/2$ and $\Delta_0 = \omega_{ac}-(\nu_1+\nu_2)/2$. The probe field frequency ν scans across the two Raman transitions. Such a gain doublet provides the negative dispersion at the center.

The susceptibility of the probe field can be written as [98]

$$\chi(\nu) = \frac{M_1}{(\nu-\nu_0-\Delta)+i\Gamma} + \frac{M_2}{(\nu-\nu_0+\Delta)+i\Gamma}, \tag{5.1}$$

where $\nu_0 = \frac{1}{2}(\nu_1+\nu_2)-\omega_{bc}$ is the probe central frequency, and Γ is the Raman transition line broadening, $M_j = N(|\mu_{ab}|^2/4\pi\hbar\epsilon_0)(|\Omega_j|^2/\Delta_0^2), (j=1,2)$ with the effective atomic number density N and dipole moment μ_{ab}. Usually we have $M_1 \cong M_2 = M$

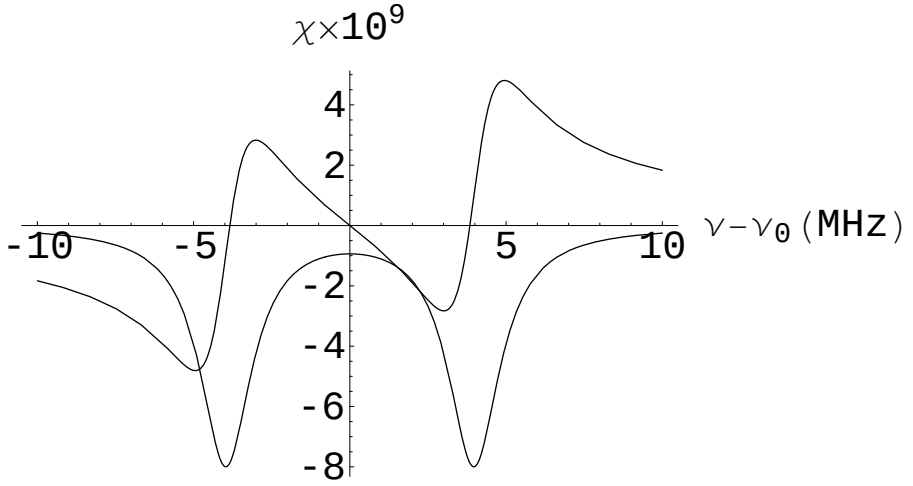

Fig. 21. The probe susceptibility of a typical bichromatic Raman system. The symmetric curve is the imaginary part and the anti-symmetric curve is the real part. The dispersion inside the gain-doublet is negative.

to get the symmetrical gain peaks. Typical susceptibility curves are shown in Fig. 21.

From the susceptibility, we can determine the refractive index n and the absorption coefficient α. At the central frequency we have

$$n \cong 1 + \frac{1}{2}\chi' = 1 + \frac{1}{2}\frac{(-M_1 + M_2)\Delta}{\Delta^2 + \Gamma^2}, \tag{5.2}$$

$$\alpha \cong \frac{\nu_0}{2c}\chi'' = -\frac{\nu_0}{2c}\frac{(M_1 + M_2)\Gamma}{\Delta^2 + \Gamma^2}, \tag{5.3}$$

where χ' and χ'' are the real and imaginary parts of the susceptibility χ. The dispersion at ν_0 is given by

$$\partial_\nu n = -\frac{M_1 + M_2}{2}\frac{(\Delta^2 - \Gamma^2)}{(\Delta^2 + \Gamma^2)^2}. \tag{5.4}$$

By choosing the parameters carefully we can have a dispersion equal to $-1/\nu_0$. Then

the white light condition is satisfied.

In order to analyze the effect of the parameter deviations, we note that M_j is proportional to both the pump field intensity I_j and the number density N. Therefore the deviations of I_j or N lead to the variation of the absorption, dispersion and refractive index as

$$\frac{\delta\left(\partial_\nu n\right)}{\partial_\nu n} = \frac{\delta\alpha}{\alpha} = \frac{\delta M_1 + \delta M_2}{2M}, \tag{5.5}$$

$$\delta n = \frac{1}{2}\frac{(-\delta M_1 + \delta M_2)\Delta}{\Delta^2 + \Gamma^2}. \tag{5.6}$$

The two intensity deviations can be independent from each other. From the proportionality between M_j and I_j we get

$$\frac{\delta\left(\partial_\nu n\right)}{\partial_\nu n} = \frac{\delta\alpha}{\alpha} = \frac{1}{2}(\frac{\delta I_1}{I_1} + \frac{\delta I_2}{I_2}). \tag{5.7}$$

It is easier to keep the white light condition if the relative intensity deviations of the two drive fields are of opposite signs.

On the other hand, number density deviation affects M_1 and M_2 simultaneously. Therefore

$$\frac{\delta\left(\partial_\nu n\right)}{\partial_\nu n} = \frac{\delta\alpha}{\alpha} = \frac{\delta N}{N}. \tag{5.8}$$

From (5.6), the refractive index does not change under the number density deviation.

Next we consider the effect of drive frequency deviation. If the frequency ν_1 is changed by the amount $\delta\nu_1$ and ν_2 is changed by $\delta\nu_2$, the susceptibility would become

$$\chi(\nu) = \frac{M}{(\nu - \nu_0 - \Delta - \delta\nu_1) + i\Gamma} + \frac{M}{(\nu - \nu_0 + \Delta - \delta\nu_2) + i\Gamma}. \tag{5.9}$$

From the susceptibility we can derive

$$\delta n = \frac{M(\Delta^2 - \Gamma^2)}{2(\Delta^2 + \Gamma^2)^2}\left(\delta\nu_1 + \delta\nu_2\right), \tag{5.10}$$

$$\delta\alpha = \frac{\nu_0 M \Delta\Gamma}{c(\Delta^2+\Gamma^2)^2}\left(\delta\nu_1 - \delta\nu_2\right), \tag{5.11}$$

$$\frac{\delta(\partial_\nu n)}{\partial_\nu n} = -\frac{\Delta(\Delta^2-3\Gamma^2)}{\Delta^4-\Gamma^4}\left(\delta\nu_1 - \delta\nu_2\right). \tag{5.12}$$

We consider the parameters from [103], i.e., $\Delta = 3.97MHz$, $\Gamma = 1MHz$ and $\lambda = 780nm$. On substituting these values into the above expressions we obtain $\delta n = 2.07\times10^{-16}(s)\left(\delta\nu_1+\delta\nu_2\right)$, $\delta\alpha = 8.97\times10^{-10}(s/m)\left(\delta\nu_1-\delta\nu_2\right)$, and $\delta(\partial_\nu n)/\partial_\nu n = -2.05\times10^{-7}(s)\left(\delta\nu_1-\delta\nu_2\right)$. Compared to the double-Λ system [88], the frequency deviation has a smaller impact to the refractive index in our system, while its effect to the dispersion and the absorption are much larger. To avoid that we can use two drive fields generated from the same laser to have the same frequency deviations. They cancel out and do not change the dispersion and absorption.

Based on the same argument as in [88] we conclude that the variation results in bichromatic Raman type white light cavity can be controlled within 10^{-4}. So in theory the white light cavity linewidth could be 10^4 times broader than an empty cavity. But of course one has to include the other imperfect effects such as the nonlinear shape of the dispersion curve, etc.

C. Effect of laser phase and amplitude noise

In the previous section, we calculated the effect of parameter deviations, or in a more strict sense, the deviation of the expectation value. Here we consider the noise effect from the drive fields. In other words, the expectation values may have satisfied the white light condition, but the random fluctuation of the laser phase and amplitude will nevertheless modify the dispersion. The phase noises account for the finite linewidth of the drive fields and the amplitude noises are responsible for the intensity

fluctuations. We calculate the effect of these noise sources independently. For simplicity, we assume that the separation between the two Raman peaks is much larger than the Raman linewidth and therefore we can treat the two Raman transitions independently.

Following the expressions in [98], the effective Hamiltonian for the system can be written as

$$\begin{aligned} \hat{H} &= \hat{H}_0 + \hat{H}_I = -\hbar\omega_{ab} \left|b\right\rangle \left\langle b\right| - \hbar\omega_{ac} \left|c\right\rangle \left\langle c\right| \\ &- \hbar\Omega_p e^{-i\nu t} \left|a\right\rangle \left\langle b\right| - \hbar\Omega_1 e^{-i\nu_1 t} \left|a\right\rangle \left\langle c\right| + H.c. \end{aligned} \tag{5.13}$$

A usual way to account for the effect of the laser phase noise is based on density matrix equations [104, 105], which is convenient if the coefficient matrices commute with each other. Here we follow a somewhat different approach as the usual methods are not easily applied. In particular, we consider the state vector instead of density matrix equations.

The state vector of the three-level atomic system is described by

$$\left|\psi\right\rangle = C_a(t) \left|a\right\rangle + C_b(t) e^{i\omega_{ab}t} \left|b\right\rangle + C_c(t) e^{i\omega_{ac}t} \left|c\right\rangle, \tag{5.14}$$

where $C_a(t)$, $C_b(t)$ and $C_c(t)$ are the slowly varying amplitudes. The equations of motion for the amplitudes of states $\left|a\right\rangle$ and $\left|b\right\rangle$ are

$$\dot{C}_a(t) = i\Omega_1 e^{-i\Delta_1 t} C_c + i\Omega_p e^{-i\Delta_p t} C_b, \tag{5.15}$$

$$\dot{C}_b(t) = i\Omega_p^* e^{i\Delta_p t} C_a - \gamma C_b, \tag{5.16}$$

where $\Delta_1 = \nu_1 - \omega_{ac}$ is the drive field detuning, $\Delta_p = \nu - \omega_{ab}$ is the probe detuning, and γ is the decay rate from level $\left|b\right\rangle$. In order to produce gain for the probe field we set the atoms to be initially in the $\left|c\right\rangle$ state. To the lowest order of approximation we

can take $C_c \approx 1$ and $C_b \approx 0$. It then follows on integrating (5.15), that

$$C_a(t) = \int_0^t i\Omega_1 e^{-i\Delta_1 t'} C_c(t') dt'. \tag{5.17}$$

From (5.16) we obtain the formal solution

$$C_b(t) = \int_0^t i\Omega_p^* e^{i\Delta_p t'} C_a(t') e^{-\gamma(t-t')} dt'. \tag{5.18}$$

The off-diagonal density matrix element ρ_{ab} is equal to (apart from the phase factor $\exp[-i\omega_{ab}t]$)

$$\begin{aligned}
\langle C_a(t) C_b^*(t) \rangle &= \int_0^t -i\Omega_p e^{-i\Delta_p t'} \langle C_a(t) C_a^*(t') \rangle e^{-\gamma(t-t')} dt' \\
&= \int_0^t -i\Omega_p e^{-i\Delta_p t'} e^{-\gamma(t-t')} dt' \int_0^t iC_c e^{-i\Delta_1 t''} dt'' \times \\
&\quad \times \int_0^{t'} -iC_c^* e^{i\Delta_1 t'''} \langle \Omega_1(t'') \Omega_1^*(t''') \rangle dt'''.
\end{aligned} \tag{5.19}$$

In order to consider the effect of phase noise, we can write the drive Rabi frequency as $\Omega_1(t) = \Omega_1 e^{i\phi_1(t)}$. As well known the phase fluctuation of a laser is a Wiener-Levy process, i.e., the random phase with Gaussian statistics performs a Brownian motion.

$$\begin{aligned}
\langle \phi_1(t) \rangle &= 0, \\
\langle \phi_1(t) \phi_1(t') \rangle &= D_1(t + t' - |t - t'|),
\end{aligned} \tag{5.20}$$

where D_1 is the phase induced bandwidth. This gives us the correlation

$$\langle \Omega_1(t) \Omega_1^*(t') \rangle = |\Omega_1|^2 \left\langle e^{i\phi_1(t) - i\phi_1(t')} \right\rangle = |\Omega_1|^2 e^{-D_1|t-t'|}. \tag{5.21}$$

On substituting from (5.21) into (5.19) we obtain

$$\langle C_a(t) C_b^*(t) \rangle \cong \frac{\Omega_p |\Omega_1|^2}{\Delta_0^2} \frac{e^{-i\Delta_p t}}{(\Delta_p - \Delta_1) + i(\gamma + D_1)} + \text{other freq.} \tag{5.22}$$

In the last step we used the far detuned condition $\Delta_0 \approx \Delta_1 \approx \Delta_p >> D_1, \gamma$ to ignore the small terms. There are also some terms with other frequencies which do not contribute to the probe susceptibility. We recall that the polarization $P = N\mu_{ab}\rho_{ab} = \chi\epsilon_0 E_p$ where the population matrix element $\rho_{ab} = \langle C_a(t)C_b^*(t)\rangle\, e^{-i\omega_{ab}t}$. Therefore with both Raman transitions the probe susceptibility under phase noises is

$$\chi(\Delta_p) = \frac{M_1}{(\Delta_p - \Delta_1) + i(\gamma + D_1)} + \frac{M_2}{(\Delta_p - \Delta_2) + i(\gamma + D_2)}. \tag{5.23}$$

This is (5.1) if we take $\Gamma_j = \gamma + D_j, (j = 1, 2)$. The inclusion of phase noise effectively increases the width of the gain peaks. From (5.4) we find that larger Γ decreases the magnitude of the dispersion. In order to keep the white light condition we can adjust the parameters. For example, we can increase the field intensity to get larger M_j, or alternatively we can use a smaller Δ. Although the dispersion condition can be restored, there is still an impact to the cavity transmission, as shown in Fig. 22. All the three curves are under white light condition with the same parameters except that Γ increases from the lowest to the highest curve. We find that the transmission bandwidth is slightly increased but the curve becomes more uneven, which is not preferred.

Next we consider the effect of amplitude noise, $\Omega_1(t) = \Omega_1 + \delta\Omega_1(t)$. The Gaussian type fluctuation can be described by an Ornstein-Uhlenbeck stochastic process [106]

$$\begin{aligned} \langle \delta\Omega_1(t)\rangle &= 0, \\ \langle \delta\Omega_1(t)\delta\Omega_1(t')\rangle &= I_{\Omega 1} A_1 e^{-A_1|t-t'|}, \end{aligned} \tag{5.24}$$

where $I_{\Omega 1}$ is the variance of amplitude fluctuations and A_1 is the amplitude fluctuation induced bandwidth. Again by substituting from (5.24) into (5.19) we obtain

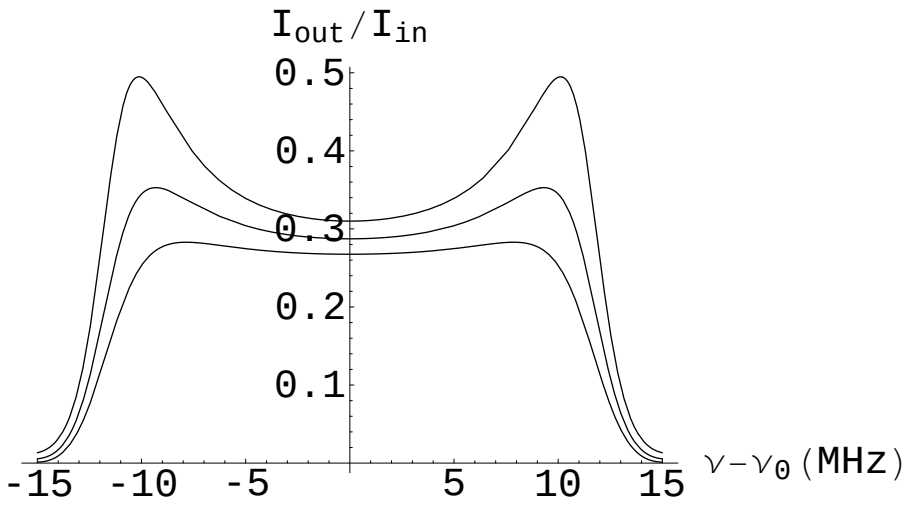

Fig. 22. The transmission curve of the white light cavity. White light condition is satisfied in all curves. The only difference is that the decay rate increases from lower curve to higher curve.

$$\begin{aligned}\langle C_a(t)C_b^*(t)\rangle &\cong \frac{\Omega_p|\Omega_1|^2}{\Delta_0^2}\frac{e^{-i\Delta_p t}}{(\Delta_p-\Delta_1)+i\gamma} \\ &+ \frac{\Omega_p I_{\Omega 1}A_1}{\Delta_0^2}\frac{e^{-i\Delta_p t}}{(\Delta_p-\Delta_1)+i(\gamma+A_1)} + \text{other freq.} \qquad (5.25)\end{aligned}$$

$$\begin{aligned}\chi(\Delta_p) &= \frac{M_1}{(\Delta_p-\Delta_1)+i\gamma} + \frac{I_{\Omega 1}A_1}{|\Omega_1|^2}\frac{M_1}{(\Delta_p-\Delta_1)+i(\gamma+A_1)} \\ &+ \frac{M_2}{(\Delta_p-\Delta_2)+i\gamma} + \frac{I_{\Omega 2}A_2}{|\Omega_2|^2}\frac{M_2}{(\Delta_p-\Delta_2)+i(\gamma+A_2)}. \qquad (5.26)\end{aligned}$$

Similarly we have ignored the small terms in (5.25). In (5.26) both Raman transitions are included to find the susceptibility under amplitude noise. The net effect are the two additional terms which are similar to the original terms with only different coefficients and γ changed to $\gamma + A_j$. Therefore both the dispersion and gain

will increase in magnitudes. Still we can satisfy the white light condition by adjusting the parameters, for example we can decrease the drive field intensity. Similarly we will find the cavity transmission curve becomes uneven since the two additional terms have a larger linewidth $\gamma + A_j$.

D. Conclusion

We consider the impact of parameter deviations and laser phase and amplitude noises on a bichromatic Raman type white light cavity. We find the dispersion, which needs to satisfy the white light condition, can be controlled within 10^{-4} under the parameter deviations. Therefore a white light cavity could have 10^4 times broader linewidth compared to an empty cavity at the same finesse.

The phase noise effectively increases the Raman linewidth by the diffusion D, causing a smaller dispersion. The amplitude noise introduces an additional term in the probe susceptibility and makes the dispersion larger. These opposite effects allow us to easily adjust the parameters to satisfy the white light condition. Both noises have the effect of making the transmission curve uneven for the white light cavity.

CHAPTER VI

REVERSING THE WEAK MEASUREMENT OF AN ARBITRARY FIELD WITH FINITE PHOTON NUMBER*

A. Introduction

In a quantum measurement, an operator projects the system into one of its eigenstates with a specific eigenvalue as the readout. Once the measurement is done, the unknown initial state of the system is destroyed, and in general there is no way to recover it from the result. However, such quantum measurement, the so-called strong or von Neumann measurement [107], is only part of the story. There is another type of quantum measurement called weak measurement [108], in which the outcome cannot determine the measured system precisely. Since this weak measurement does not totally *collapse* the system, the information of the initial state can be passed over to the final state. If such retained information is complete, it would be possible to recover the initial state with some operations. This kind of state protection could be useful for quantum information processing.

One type of reversible measurements is deterministic, in which the initial state lies in a certain subspace and the measurement provides no information about it. Mabuchi and Zoller showed the conditions to unitarily invert quantum jumps in continuously monitored systems [109]. These conditions have been generalized by Nielsen and Caves to any ideal quantum operation [110], with quantum teleportation as a special

*Reprinted with permission from "Reversing the weak measurement of an arbitrary field with finite photon number" by Q. Sun, M. Al-Amri, and M. S. Zubairy, 2009. *Phys. Rev. A*, vol. 80, pp. 033838, Copyright [2009] by the American Physical Society.

example.

Another type is the probabilistically reversible measurements, for which only a certain outcome of the second measurement successfully restores the initial state. It has been discussed in quantum counter [111], quantum nondemolition measurement [112], spin systems [113], and linear optics [114]. A general theory with necessary and sufficient conditions has been given in [115] as well as an information-theoretical analysis in [116]. Koashi and Ueda derived a trade-off relation between the unsharpness of the measurement and the best efficiency of the reversing operation [117]. In a recent experiment [118], based on a proposal by Korotkov and Jordan [119], the reversal of a weak measurement on a superconducting phase qubit was performed. A general procedure for N-dimensional system was also proposed in [119], which requires 2^N steps.

An important question remains: can we reverse a multi-dimensional state in a simpler way? In Section B, we address this question and propose two schemes in cavity quantum electrodynamics (QED) systems, in which only a few steps are needed for the reversal. In Section C, we further consider click-allowed reversal for a specific class of states. Section D is the conclusion.

B. Schemes

The state is an arbitrary cavity field with finite photon number $\sum_{n,m=0}^{n_{\max}} \rho_{nm} |n\rangle \langle m|$, which is continuously monitored by an ideal photon detector outside. If there is no click, the field evolves into $\sum_{n,m=0}^{n_{\max}} \rho_{nm} e^{-(n+m)\gamma t} |n\rangle \langle m|$ according to the quantum trajectory theory, where 2γ is the photon decay rate in the cavity and t is the duration of the measurement. Here we ignore all the normalization constants for simplicity till the end of the derivation. For finite time this measurement is not sharp since any

Fock component could give null result. To reverse the weak measurement, we need to swap the components symmetrically to $\sum_{n,m=0}^{n_{\max}} \rho_{nm} e^{-(n+m)\gamma t} |N-n\rangle \langle N-m|$, where $N(\geq n_{\max})$ is an adjustable system parameter. Then we make another measurement. If it successfully produces null result again, the resulting field is projected into $\sum_{n,m=0}^{n_{\max}} \rho_{nm} e^{-2N\gamma t} |N-n\rangle \langle N-m|$. The common factor $e^{-2N\gamma t}$ is dropped after normalization. Finally we swap back the components and the initial field is restored.

So the main challenge is how to swap the components $|n\rangle \rightarrow |N-n\rangle$ for all $n \in [0, n_{\max}]$ simultaneously. In our schemes, we realize it by using either multiple atoms or an atom with degenerate sublevels. Both schemes adopt the adiabatic passages to map the field coherence into the atoms, then swap the atomic levels with the help of some auxiliary fields, and finally map the coherence back to the field. The swapping procedures for each scheme go as following:

1. Multi-atom scheme

The atoms are Λ-type with an excited level $|a\rangle$ and two lower levels $|b\rangle$ and $|c\rangle$. We prepare $N(\geq n_{\max})$ atoms in level $|c\rangle$ and send them into the cavity. The diagram of the scheme is shown in Fig. 23. Two classical fields transversely propagate through two sides of the cavity. They are both resonant to the transition $|b\rangle \leftrightarrow |a\rangle$ and have space-dependent Rabi frequencies $\Omega(z)$ and $\Omega'(z)$, where z is the longitudinal coordinate. The cavity mode in the middle is resonant to the transition $|c\rangle \leftrightarrow |a\rangle$ with a coupling constant $g(z)$. To verify that the scheme works, we consider a Fock component $|n\rangle$ of the field.

Step (I) At the entrance the atoms encounter first the classical field $\Omega(z)$ and then the cavity mode $g(z)$. The Hamiltonian of the system can be written as [14]

$$H = \sum_{i=1}^{N} (\hbar\Omega |a_i\rangle \langle b_i| + \hbar g |a_i\rangle \langle c_i| \hat{a}) + H.c. \tag{6.1}$$

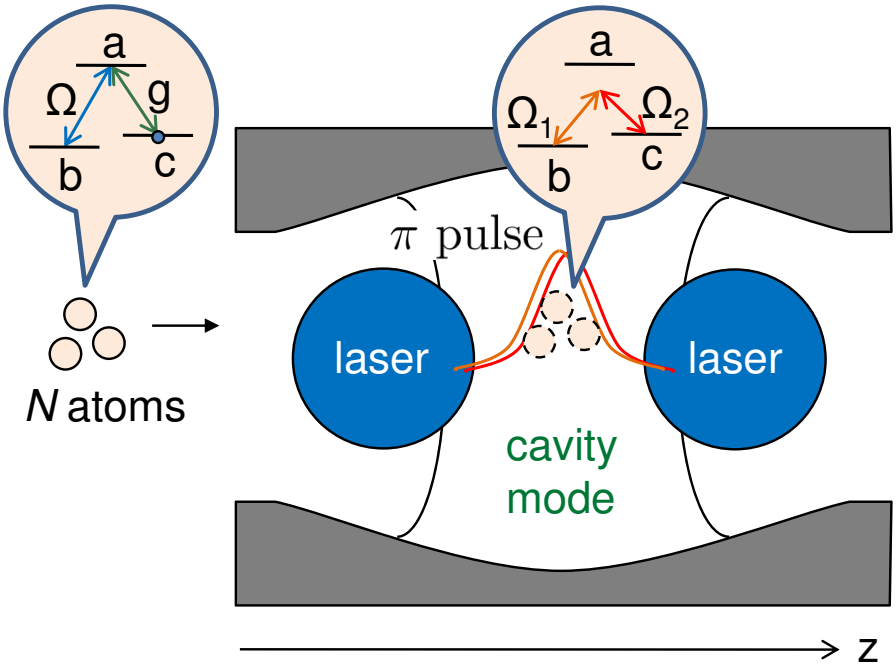

Fig. 23. The multi-atom scheme. An adiabatic passage maps the field state into the atoms. Then the atomic levels are swapped by an effective π pulse. Finally another adiabatic passage maps the state back to the cavity field.

where $\hat{a}$ is the annihilation operator for the cavity mode. Such a system has a manifold of dark states [120], which evolve in parallel. Each number of excitations, either in the form of cavity mode photons or level $|b\rangle$ atoms, has its own dark state. The one with $n(\leq N)$ excitations is

$$\begin{aligned}\left|\Psi_n^{\text{dark}}\right\rangle &= (-\Omega/g)^n \left|c\cdots c\right\rangle \left|n\right\rangle / \sqrt{n!} \\ &+(-\Omega/g)^{n-1} \sum_{i=1}^{N} \left|c\cdots b_i \cdots c\right\rangle \left|n-1\right\rangle / \sqrt{(n-1)!} \\ &+\cdots+ \sum_{1\leq i_1<\cdots<i_n\leq N} \left|c\cdots b_{i_1}\cdots b_{i_n}\cdots c\right\rangle \left|0\right\rangle . \end{aligned} \tag{6.2}$$

The key to state mapping is the adiabatic passage within the dark states. When the atoms move from the classical field region into the cavity mode region, they feel

the adiabatic change from $\Omega \gg g$ to $\Omega \ll g$. The component evolves as:

$$|c\cdots c\rangle\,|n\rangle \rightarrow \sum_{1\leq i_1<\cdots<i_n\leq N} |c\cdots b_{i_1}\cdots b_{i_n}\cdots c\rangle\,|0\rangle\,. \tag{6.3}$$

Phase factor from $(-\Omega/g)^n$ is neglected here because it will be cancelled after the reversal.

Step (II) We add two other classical fields to the middle of the cavity. They have the same detuning $\nu_1 - \omega_{ab} = \nu_2 - \omega_{ac} = \Delta$ and same Rabi frequency $\Omega_1 = \Omega_2 \ll \Delta$. Under the initial condition $c_a(0) \approx 0$, the excited level is adiabatically eliminated and each atom effectively behaves like a two-level atom. The two lower levels swap with each other after a π pulse, $|b\rangle \leftrightarrow -|c\rangle$. So the component changes as

$$\sum_{1\leq i_1<\cdots<i_n\leq N} |c\cdots b_{i_1}\cdots b_{i_n}\cdots c\rangle\,|0\rangle \rightarrow \sum_{1\leq i_1<\cdots<i_{N-n}\leq N} \left|b_{i_1}\cdots c\cdots c\cdots b_{i_{N-n}}\right\rangle|0\rangle\,, \tag{6.4}$$

which is just another dark state with $N-n$ excitations.

Step (III) Now the atoms leave the cavity mode and encounter the other resonant classical field $\Omega'(z)$. They feel the adiabatic change from $\Omega' \ll g$ to $\Omega' \gg g$, the dark states evolve as the reversal of (6.3):

$$\sum_{1\leq i_1<\cdots<i_{N-n}\leq N} \left|b_{i_1}\cdots c\cdots b_{i_{N-n}}\right\rangle|0\rangle \rightarrow |c\cdots c\rangle\,|N-n\rangle\,. \tag{6.5}$$

So after the atoms fly out, the coherence is mapped back to the field, and the swapping $|n\rangle \rightarrow |N-n\rangle$ is achieved.

2. Zeeman-level scheme

The second scheme uses a degenerate two-level atom with $J_g = N+1 \leftrightarrow J_e = N$. We send in the atom prepared in the level $|g_N\rangle$. The diagram of the scheme is shown in Fig. 24(d). Two circularly polarized classical fields are placed at two sides of the cavity with the π polarized cavity mode in the middle. They are all resonant to the

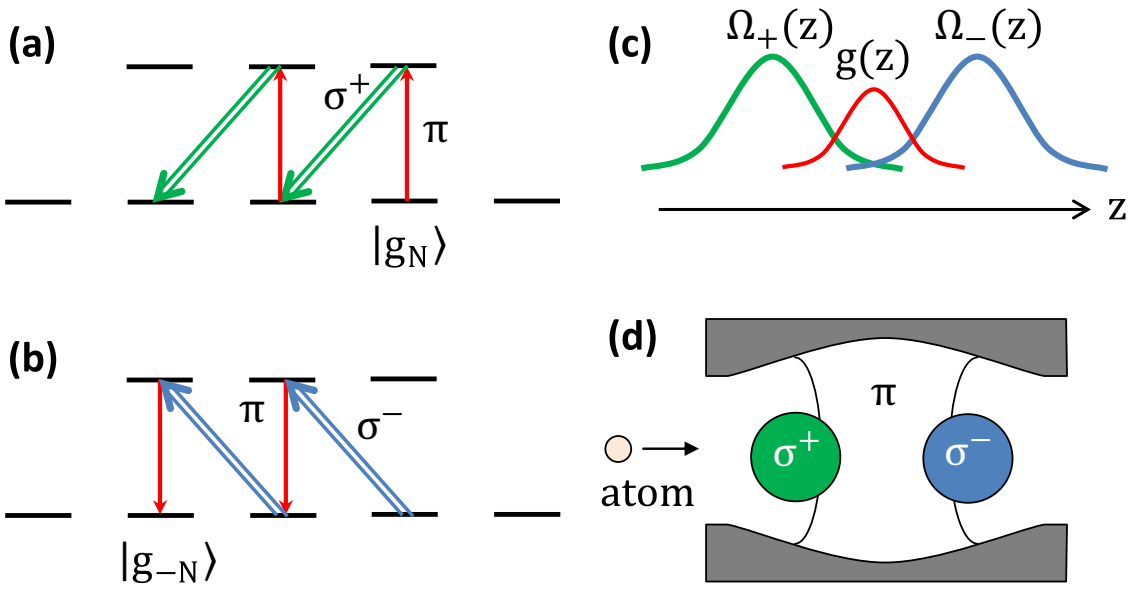

Fig. 24. The Zeeman-level scheme. (a) Level structure in Step (I). The classical field is σ^+ polarized and the cavity mode is π polarized. (b) Level structure in Step (II). The classical field is σ^- polarized. (c) The profiles of the fields, required for the adiabatic passages. (d) The system diagram.

atomic separation and the Rabi frequencies are $\Omega_+(z)$, $\Omega_-(z)$, and $g(z)$, respectively. We examine the transformation of an arbitrary field component $|n\rangle$ below.

Step (I) The atom first encounters the σ^+ field and then the cavity mode, with the level structure shown in Fig. 24(a). The dark state containing the component $|g_N\rangle\,|n\rangle$ is [121, 122]

$$\begin{aligned}\left|\Psi^{\rm dark}_{n,g_N}\right\rangle &= |g_N\rangle\,|n\rangle\,\Omega_N\Omega_{N-1}\cdots\Omega_{N-n+1}\\ &+ |g_{N-1}\rangle\,|n-1\rangle\,G^{(n)}_N\Omega_{N-1}\cdots\Omega_{N-n+1}\\ &+ \cdots + |g_{N-n}\rangle\,|0\rangle\,G^{(n)}_N G^{(n)}_{N-1}\cdots G^{(n)}_{N-n+1},\end{aligned} \tag{6.6}$$

where $G^{(n)}_k = g(t)\sqrt{n+k-N}\,\langle J_g(m_g=k);10|J_e(m_e=k)\rangle$, and the Rabi frequencies $\Omega_k = \Omega_+(t)\,\langle J_g(m_g=k-1);11|J_e(m_e=k)\rangle$. For this configuration all the Clebsch-

Gordan coefficients are nonzero. So when leaving the σ^+ field and entering the cavity mode, the atom feels the adiabatic change from $\Omega_+ \gg g$ to $\Omega_+ \ll g$ and the state transforms as

$$|g_N\rangle |n\rangle \rightarrow |g_{N-n}\rangle |0\rangle , \tag{6.7}$$

under the condition $n_{\max} \leq 2N$. The atom jumps to the left sublevels, consuming one photon at each jump.

Step (II) In the latter half of the cavity, the atom only feels the cavity mode and the σ^- polarized field, as shown in Fig. 24(b). The new dark states are very similar to (6.6), except that now they connect all the ground levels to $|g_{-N}\rangle$. When the atom moves from the cavity mode to the σ^- field, it feels the change from $\Omega_- \ll g$ to $\Omega_- \gg g$. The adiabatic passage pumps the atom toward the left sublevels, generating one photon at each jump. In the end the state transforms as

$$|g_{N-n}\rangle |0\rangle \rightarrow |g_{-N}\rangle |2N-n\rangle . \tag{6.8}$$

Then we remove the atom and the remaining field is $|2N-n\rangle$.

We immediately find the advantage of this scheme: the fixed total number of jumps ($2N$) automatically swaps the components when we map the state back to the field, so only two steps are required instead of three in the first scheme. Another advantage is that it does not require precise interaction time since there is no π pulse.

3. Probability and information analysis

The reversing probability is just the probability of null result during the second measurement, which can be written as

$$P_2^{(0)}(t) = \frac{\mathrm{Tr}(\sum_{n,m=0}^{n_{\max}} \rho_{nm} e^{-2N\gamma t} |N-n\rangle \langle N-m|)}{\mathrm{Tr}(\sum_{n,m=0}^{n_{\max}} \rho_{nm} e^{-(n+m)\gamma t} |N-n\rangle \langle N-m|)}$$

$$= \quad e^{-2N\gamma t} / \sum_{n=0}^{n_{\max}} e^{-2n\gamma t} \rho_{nn}. \tag{6.9}$$

(or $N \to 2N$ for the second scheme). In order to increase the success probability we should choose small N, down to the limit $N = n_{\max}$, in which case the probability is optimal because it reaches the upper bound $\min P^{(0)}/P^{(0)}(\rho)$ [119]. Since $e^{-2N\gamma t}$ decreases faster than any term in the denominator, $P_2^{(0)}(t)$ decreases with time.

From the information-theoretical point of view, we can take the field being in state $|n\rangle$ as an event $x_n \in X$, and the detector reading of k clicks as $y_k \in Y$. The mutual information gained from the first null-result measurement can be written as [123],

$$I(X; y_0) \quad = \quad \sum_{n=0}^{n_{\max}} p(x_n|y_0) \log \frac{p(x_n|y_0)}{p(x_n)}, \tag{6.10}$$

where $p(x_n) = \rho_{nn}$ is the initial probability, and $p(x_n|y_0) = e^{-2n\gamma t}\rho_{nn} / \sum_{n'=0}^{n_{\max}} e^{-2n'\gamma t}\rho_{n'n'}$ is the final probability for the field to be in $|n\rangle$. From Cauchy inequality we find $dI/dt > 0$ for all $t \in (0, \infty)$. The two limits are $I(0) = 0$ which means no measurement (weakest), and $I(\infty) = -\log\rho_{00}$ which means a sharp measurement. So for a longer monitoring time, the measurement is stronger and more information is gained, while the reversing probability decreases. We illustrate these trends with a simple example as shown in Fig. 25.

C. Click-allowed reversal

So far we have been considering the reversibility of null-result measurements. Such measurements do not destroy any component and only generate exponential factors which can be unified by a symmetric swapping and another null measurement. In the situation of photons being detected, the annihilation operator could destroy some components and it also brings additional factors which cannot be unified in gen-

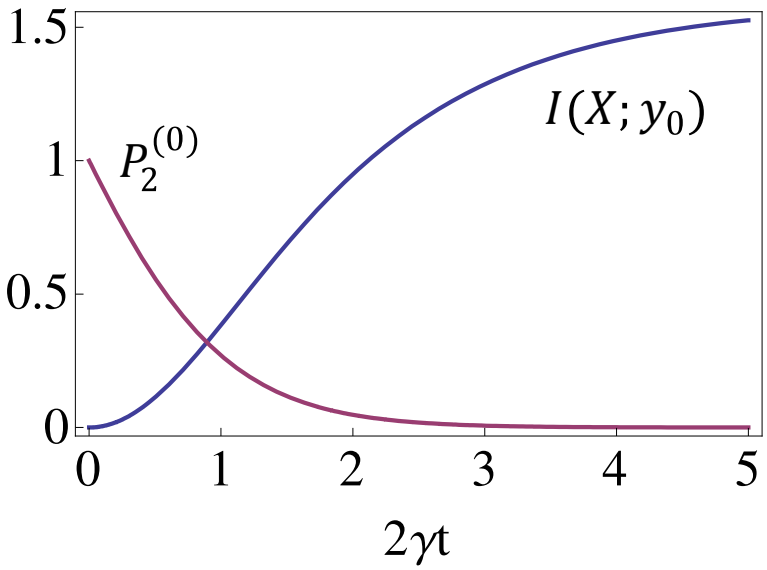

Fig. 25. The reversal probability and gained information curves. The initial state is $(|0\rangle + |1\rangle + |2\rangle)/\sqrt{3}$. With the time passing by, more information $I(X;y_0)$ is obtained while the chance of successful reversal $P_2^{(0)}$ diminishes.

eral. Only a certain class of states, namely the two-component states $\rho_{nn}|n\rangle\langle n| + \rho_{mm}|m\rangle\langle m| + \rho_{nm}|n\rangle\langle m| + \rho_{mn}|m\rangle\langle n|$, can still be reversed probabilistically. If the photon detector registered k ($m > n \geq k$) clicks during time t, the component $|n\rangle$ will change into

$$e^{-\gamma\hat{a}^\dagger\hat{a}t}\hat{a}^k|n\rangle = e^{-\gamma(n-k)t}\sqrt{n!/(n-k)!}\,|n-k\rangle\,, \tag{6.11}$$

where we have ignored the pre-factor $e^{-\gamma(t_1+\cdots+t_k)}$ because it will be cancelled after normalization. To reverse this measurement, we adopt the swapping procedures described in the two schemes. Taking N (or $2N$ in the second scheme) $= m + n - k$, the component after swapping would be $e^{-\gamma(n-k)t}\sqrt{n!/(n-k)!}\,|m\rangle$. After another measurement, provided there are k clicks as well, we swap again and the component becomes $e^{-\gamma(n-k)t}\sqrt{n!/(n-k)!}e^{-\gamma(m-k)t}\sqrt{m!/(m-k)!}\,|n\rangle$. The initial $|m\rangle$ component

will have the same factor which is symmetric to m and n. So the normalized field is identical to the initial one.

The probability of k clicks during the first measurement is

$$P_1^{(k)}(t) = (1 - e^{-2\gamma t})^k \left[\binom{m}{k} e^{-2\gamma(m-k)t} \rho_{mm} + \binom{n}{k} e^{-2\gamma(n-k)t} \rho_{nn} \right]. \tag{6.12}$$

The physical meaning is clear: for a Fock state $|n\rangle$ to have k clicks within time t, the photons have to be separated into two groups which causes the combination factor $\binom{n}{k}$. Each of the remaining $n-k$ photons contributes a factor $e^{-2\gamma t}$, and each of the decayed k photons contributes a factor $1 - e^{-2\gamma t}$. The reversing probability is the probability of emitting k photons in the second measurement. Following the same argument, we find it to be

$$P_2^{(k)}(t) = (e^{2\gamma t} - 1)^k \frac{\binom{m}{k} e^{-2\gamma m t} \binom{n}{k} e^{-2\gamma n t}}{\binom{m}{k} e^{-2\gamma m t} \rho_{mm} + \binom{n}{k} e^{-2\gamma n t} \rho_{nn}}. \tag{6.13}$$

When $k = 0$, the above equation reduces to (6.9).

The advantage of click-allowed reversal is clear when we consider the probability of state protection. $P_1^{(k)}(t) P_2^{(k)}(t)$ gives the protection probability along the k-click path. So the total probability of protecting a field with two components $|m\rangle$ and $|n\rangle$ in time $2t$ is

$$\begin{aligned} P_s(2t) &= \sum_{k=0}^{n} P_1^{(k)}(t) P_2^{(k)}(t) \\ &= e^{-2\gamma(m+n)t} \sum_{k=0}^{n} (e^{2\gamma t} - 1)^{2k} \binom{m}{k} \binom{n}{k}. \end{aligned} \tag{6.14}$$

We can choose $n = m - 1$ to optimize the result.

For the no-click reversal of a general state $\sum_{n,m=0}^{n_{\max}} \rho_{nm} |n\rangle \langle m|$, the probability of null result during the first measurement is $P_1^{(0)}(t) = \sum_{n=0}^{n_{\max}} e^{-2n\gamma t} \rho_{nn}$. Therefore the

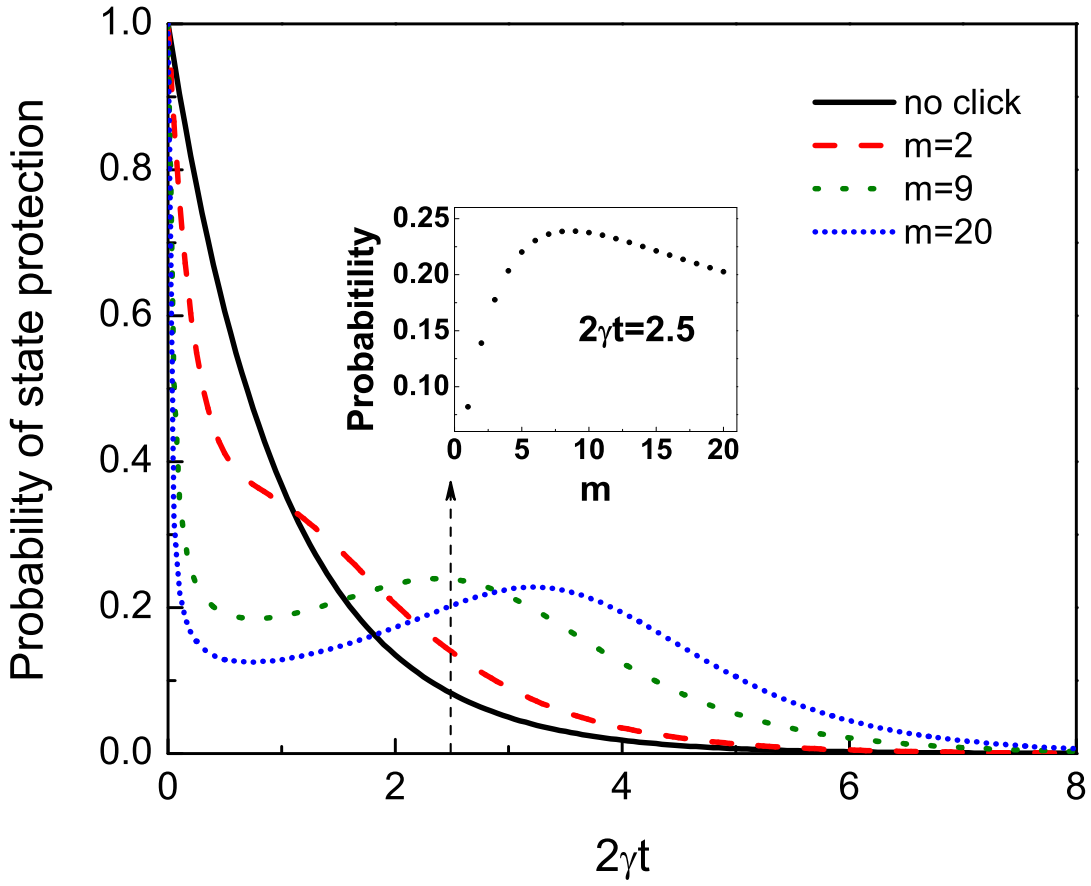

Fig. 26. The state protection probability-time curves for no-click reversal, and click--allowed reversals with $m = 2, 9, 20 (n \equiv m - 1)$. (inset) The probability-m relation for a fixed $2\gamma t = 2.5$.

protection probability is

$$P_s^{(0)}(2t) = P_1^{(0)}(t) P_2^{(0)}(t) = e^{-2N\gamma t}, \tag{6.15}$$

which is highest when we take $N = n_{\max} = 1$. Interestingly, both $P_s(2t)$ and $P_s^{(0)}(2t)$ are independent of the initial coefficients. Their comparison is shown in Fig. 26. The no-click reversal has higher protection probability for short time, while the click-allowed reversal is more successful for long time protection. This trend is more obvious

for larger m as those curves are more extended in the time domain. For a specific time we can find out which m gives the best probability, as shown in Fig. 26(inset). Even for $2\gamma t = 5$ when the no-click reversal gives a protection probability of only 0.0067, the click-allowed reversal can still have a success chance above 0.2, although the m required is around 100 which is quite a challenge. In case of a limited m, the long-time protection probability will be low. But we can increase it by split the time into many shorter cycles of measurement and reversal.

D. Conclusion

In summary, we propose two schemes to reverse the weak measurement of arbitrary states with finite photons. Taking advantage of the adiabatic passage in the dark states, the reversal can be achieved in a few simple steps. We also consider the click-allowed reversal for a certain class of states and show its advantage in state protection.

In all the derivations above, we assumed that the photon decay during the swapping procedures is negligible. This requires the adiabatic passage to be much faster than the typical photon decay time, i.e., $1/T \gg \gamma$. The condition for adiabatic passage $g, \Omega \gg 1/T$ also needs to be satisfied. The atomic decay can be neglected because the excited levels are never significantly populated. Another issue is the overall phase of the state, which may not be reversible. It could have an effect for applications like interferometry.

The implementation of the first scheme could benefit a lot from the fact that experimentalists have been playing with Λ-type three-level atoms for a long time. For the second scheme, the degenerate two-level atom has many possible candidates, such as the transition $2p^5 3s(^3P_2) \rightarrow 2p^5 3p(^3P_1)$ in neon [124] and $1s_5(J = 2) \rightarrow$

$2p_{10}(J = 1)$ in argon [125]. There are also several techniques to prepare the atom into a Zeeman sublevel, see [126] and the references therein.

CHAPTER VII

SUMMARY

In summary, we have studied the coherent atomic effects and their applications in many systems. Most of these effects are based on EIT. Using the steep positive dispersion of EIT, we proposed a scheme for broadband slow light propagation. The pulse is frequency decomposed and each frequency goes through its own EIT window shifted by the magnetic field gradient. Using the refractive index near transparency, we suggested a scheme for optical beam steering. The drive field intensity gradient leads to a refractive index gradient, which deflects the light. We found the optimal drive field profiles for single frequency deflection and beam focusing, and we found that the previous scheme is good for broadband pulse deflection. Even the absorption of EIT can be very useful. We considered the effect of putting an EIT medium into a laser cavity. If the drive field is strong, the EIT medium is almost transparent and the laser system goes through second-order phase transition. But if the drive field is very weak, the EIT medium acts like a saturable absorber and the system goes through first-order phase transition.

We have also studied other coherent effects besides EIT. We analyzed the effects of noise and parameter deviations in a bichromatic Raman type white light cavity. In such a cavity a continuous range of frequencies can be resonant at the same time due to the negative dispersion which compensates the phase delay difference. Finally by making use of STIRAP, we proposed two schemes to reverse the weak measurement of an arbitrary field with finite photon number.

REFERENCES

[1] G. Alzetta, A. Gozzini, L. Moi, and G. Orriols, "An experimental method for the observation of r.f. transitions and laser beat resonances in oriented Na vapour," *Nuovo Cimento Soc. Ital. Fis., B*, vol. 36, no. 1, pp. 5-20, 1976.

[2] R. M. Whitley and C. R. Stroud, "Double optical resonance," *Phys. Rev. A*, vol. 14, no. 4, pp. 1498-1513, 1976.

[3] E. Arimondo and G. Orriols, "Nonabsorbing atomic coherences by coherent two-photon transitions in a three-level optical pumping," *Lettere al Nuovo Cimento*, vol. 17, no. 10, pp. 333-338, 1976.

[4] S. E. Harris, J. E. Field, and A. Imamoglu, "Nonlinear optical processes using electromagnetically induced transparency," *Phys. Rev. Lett.*, vol. 64, no. 10, pp. 1107-1110, 1990.

[5] K. H. Hahn, D. A. King, and S. E. Harris,"Nonlinear generation of 104.8-nm radiation within an absorption window in zinc," *Phys. Rev. Lett.*, vol. 65, no. 22, pp. 2777-2779, 1990.

[6] K.-J. Boller, A. Imamoglu, and S. E. Harris, "Observation of electromagnetically induced transparency," *Phys. Rev. Lett.*, vol. 66, no. 20, pp. 2593-2596, 1991.

[7] A. Kasapi, M. Jain, G. Y. Yin, and S. E. Harris, "Electromagnetically induced transparency: Propagation dynamics," *Phys. Rev. Lett.*, vol. 74, no. 13, pp. 2447-2450, 1995.

[8] O. Schmidt, R. Wynands, Z. Hussein and D. Meschede, "Steep dispersion and group velocity below c/3000 in coherent population trapping," *Phys. Rev. A*, vol. 53, no. 1, pp. R27-R30, 1996.

[9] M. M. Kash, V. A. Sautenkov, A. S. Zibrov, L. Hollberg, G. R. Welch, M. D. Lukin, Y. Rostovtsev, E. S. Fry and M. O. Scully, "Ultraslow group velocity and enhanced nonlinear optical effects in a coherently driven hot atomic gas," *Phys. Rev. Lett.*, vol. 82, no. 26, pp. 5229-5232, 1999.

[10] L. V. Hau, S. E. Harris, Z. Dutton and C. H. Behroozi, "Light speed reduction to 17 metres per second in an ultracold atomic gas," *Nature*, vol. 397, pp. 594-598, 1999.

[11] D. Budker, D. F. Kimball, S. M. Rochester and V. V. Yashchuk, "Nonlinear magneto-optics and reduced group velocity of light in atomic vapor with slow ground state relaxation," *Phys. Rev. Lett.*, vol. 83, no. 9, pp. 1767-1770, 1999.

[12] C. LiuZ. Dutton, C. H. Behroozi and L. V. Hau, "Observation of coherent optical information storage in an atomic medium using halted light pulses," *Nature*, vol. 409, pp. 490-493, 2001.

[13] M. O. Scully, "Enhancement of the index of refraction via quantum coherence," *Phys. Rev. Lett.*, vol. 67, no. 14, pp. 1855-1858, 1991.

[14] M. O. Scully and M. S. Zubairy, *Quantum Optics*. New York: Cambridge University Press, 1997.

[15] T. Kamiya, F. Saito, O. Wada, and H. Yajima, *Femtosecond Technology*. Berlin: Springer, 1999.

[16] S. E. Harris and L. V. Hau, "Nonlinear optics at low light levels," *Phys. Rev. Lett.*, vol. 82, no. 23, pp. 4611-4614, 1999.

[17] P. C. Ku, C. J. Chang-Hasnain, and S. L. Chuang, "Variable semiconductor all-optical buffer," *Electron. Lett.*, vol. 38, no. 24, pp. 1581-1583, 2002.

[18] A. V. Turukhin, V. S. Sudarshanam. M. S. Shahriar, J. A. Musser, B. S. Ham, P. R. Hemmer, "Observation of ultraslow and stored light pulses in a solid," *Phys. Rev. Lett.*, vol. 88, no. 2, pp. 023602, 2001.

[19] M. S. Bigelow, N. N. Lepeshkin, R. W. Boyd, "Observation of ultraslow light propagation in a ruby crystal at room temperature," *Phys. Rev. Lett.*, vol. 90, no. 11, pp. 113903, 2003.

[20] A. B. Matsko, O. Kocharovskaya, Y. Rostovtsev, G. R. Welch, A. S. Zibrov, M. O. Scully, "Slow, ultraslow, stored, and frozen light," in *The Advances in Atomic, Molecular, and Optical Physics*, B. Bederson and H. Walther, Eds. San Diego: Academic, 2001, vol. 46, pp. 191-242.

[21] M. Born and E. Wolf, *Principles of Optics*. New York: Cambridge University Press, 1999.

[22] Z. Dutton, M. Bashansky, M. Steiner, J. Reintjes, "Channelization architecture for wide-band slow light in atomic vapors," in *Proc. SPIE (Advanced Optical and Quantum Memories and Computing II)*, San Jose, CA, Jan. 2005, vol. 5735, pp. 115-129.

[23] Z. Deng, D.-K. Qing, P. Hemmer, C. H. R. Ooi, M. S. Zubairy, and M. O. Scully, "Time-bandwidth problem in room temperature slow light," *Phys. Rev. Lett.*, vol. 96, no. 2, pp. 023602, 2006.

[24] A. B. Matsko, D. V. Strekalov, L. Maleki, "On the dynamic range of optical delay lines based on coherent atomic media," *Opt. Express*, vol. 13, no. 6, pp. 2210-2223, 2005.

[25] R. W. Boyd, D. J. Gauthier, A. L. Gaeta, A. E. Willner, "Maximum time delay

achievable on propagation through a slow-light medium," *Phys. Rev. A*, vol. 71, no. 2, pp. 023801, 2005.

[26] V. J. Fowler and J. Schlafer, "A survey of laser beam deflection techniques," *Appl. Opt.*, vol. 5, no. 10, pp. 1675-1682, 1966.

[27] M. Gottlieb, C. L. M. Ireland, and J. M. Ley, *Electro-Optic and Acousto-Optic Scanning and Deflection*. New York: Dekker, 1983.

[28] I. Cindrich, "Image scanning by rotation of a hologram," *Appl. Opt.*, vol. 6, no. 9, pp. 1531-1534, 1967.

[29] D. H. McMahon, A. R. Franklin, and J. B. Thaxter, "Light beam deflection using holographic scanning techniques," *Appl. Opt.*, vol. 8, no. 2, pp. 399-402, 1969.

[30] P. J. Brosens, "Fast retrace optical scanning," *Electro-Opt. Syst. Des.*, vol. 3, no. 4, pp. 21-24, 1971.

[31] W. B. Jackson, N. M. Amer, A. C. Boccara, and D. Fournier, "Photothermal deflection spectroscopy and detection," *Appl. Opt.*, vol. 20, no. 8, pp. 1333-1344, 1981.

[32] R. W. Dixon, "Photoelastic properties of selected materials and their relevance for applications to acoustic light modulators and scanners," *J. Appl. Phys.*, vol. 38, no. 13, pp. 5149-5153, 1967.

[33] D. A. Pinnow, "Guide lines for the selection of acoustooptic materials," *IEEE J. Quantum ELectron.*, vol. QE-6, no. 4, pp. 223-238, 1970.

[34] E. G. Spencer, P. V. Lenzo, and A. A. Ballman, "Dielectric materials for electrooptic, elastooptic, and ultrasonic device applications," *Proc. IEEE*, vol. 55, no. 12, pp. 2074-2104, 1967.

[35] T. C. Lee and J. D. Zook, "Light beam deflection with electrooptic prisms," *IEEE J. Quantum ELectron.*, vol. QE-4, no. 7, pp. 442-454, 1968.

[36] J. F. Lotspeich, "Electrooptic light-beam deflection," *IEEE Spectrum*, vol. 5, no. 2, pp. 45-52, 1968.

[37] J. D. Zook, "Light beam deflector performance: A comparative analysis," *Appl. Opt.*, vol. 13, no. 4, pp. 875-887, 1974.

[38] H. Kosaka, T. Kawashima, A. Tomita, M. Notomi, T. Tamamura, T. Sato, and S. Kawakami, "Superprism phenomena in photonic crystals," *Phys. Rev. B*, vol. 58, no. 16, pp. R10096-R10099, 1998.

[39] T. Baba and M. Nakamura, "Photonic crystal light deflection devices using the superprism effect," *J. Quantum Electron.*, vol. 38, no. 7, pp. 909-914, 2002.

[40] F. Vasey, F. K. Reinhart, R. Houdre, and J. M. Stauffer, "Spatial optical beam steering with an algaas integrated phased array," *Appl. Opt.*, vol. 32, no. 18, pp. 3220-3232, 1993.

[41] M. W. Farn, "Agile beam steering using phased-arraylike binary optics," *Appl. Opt.*, vol. 33, no. 22, pp. 5151-5158, 1994.

[42] S. Ahderom, M. Raisi, K. Lo, K. E. Alameh, and R. Mavaddat, "Applications of liquid crystal spatial light modulators in optical communications," in *Proc. SPIE (5th Int. Conf. High-Speed Networks and Multimedia Communications)*, Jeju Island, Korea, Jul. 2002, pp. 239-242.

[43] A. C. Tam and W. Happer, "Long-range interactions between cw self-focused laser beams in an atomic vapor," *Phys. Rev. Lett.*, vol. 38, no. 6, pp. 278-282, 1977.

[44] G. T. Purves, G. Jundt, C. S. Adams, and I. G. Hughes, "Refractive index measurements by probe-beam deflection," *Eur. Phys. J. D*, vol. 29, no. 3, pp. 433-436, 2004.

[45] M. O. Scully and S. Y. Zhu, "Ultra-large index of refraction via quantum interference," *Opt. Comm.*, vol. 87, no. 3, pp. 134-138, 1992.

[46] M. Xiao, Y. Q. Li, S. Z. Jin, and J. Gea-Banacloche, "Measurement of dispersive properties of electromagnetically induced transparency in rubidium atoms," *Phys. Rev. Lett.*, vol. 74, no. 5, pp. 666-669, 1995.

[47] R. R. Moseley, S. Shepherd, D. J. Fulton, B. D. Sinclair, and M. H. Dunn, "Spatial consequences of electromagnetically induced transparency: Observation of electromagnetically induced focusing," *Phys. Rev. Lett.*, vol. 74, no. 5, pp. 670-673, 1995.

[48] R. R. Moseley, S. Shepherd, D. J. Fulton, B. D. Sinclair, and M. H. Dunn, "Electromagnetically-induced focusing," *Phys. Rev. A*, vol. 53, no. 1, pp. 408-415, 1996.

[49] M. Mitsunaga, M. Yamashita, and H. Inoue, "Absorption imaging of electromagnetically induced transparency in cold sodium atoms," *Phys. Rev. A*, vol. 62, no. 1, pp. 013817, 2000.

[50] A. G. Truscott, M. E. J. Friese, N. R. Heckenberg, and H. Rubinsztein-Dunlop, "Optically written waveguide in an atomic vapor," *Phys. Rev. Lett.*, vol. 82, no. 7, pp. 1438-1441, 1999.

[51] J. A. Andersen, M. E. J. Friese, A. G. Truscott, Z. Ficek, P. D. Drummond, N. R. Heckenberg, and H. Rubinsztein-Dunlop, "Light guiding light: Nonlinear

refraction in rubidium vapor," *Phys. Rev. A*, vol. 63, no. 2, pp. 023820, 2001.

[52] R. Kapoor and G. S. Agarwal, "Theory of electromagnetically induced waveguides," *Phys. Rev. A*, vol. 61, no. 5, pp. 053818, 2000.

[53] A. Y. Savchencko and B. Y. Zel'dovich, "Wave propagation in a guiding structure: Beyond the paraxial approximation one step," *J. Opt. Soc. Am. B*, vol. 13, no. 2, pp. 273-281, 1996.

[54] A. Ciattoni, P. D. Porto, B. Crosignani, and A. Yariv, "Vectorial nonparaxial propagation equation in the presence of a tensorial refractive-index perturbation," *J. Opt. Soc. Am. B*, vol. 17, no. 5, pp. 809-819, 2000.

[55] Q. Sun, Y. V. Rostovtsev, J. P. Dowling, M. O. Scully, and M. S. Zubairy, "Optically controlled delays for broadband pulses," *Phys. Rev. A*, vol. 72, no. 3, pp. 031802(R), 2005.

[56] V. DeGiorgio and M. O. Scully, "Analogy between the laser threshold region and a second-order phase transition," *Phys. Rev. A*, vol. 2, no. 4, pp. 1170-1177, 1970.

[57] R. Graham and H. Haken, "Laserlight - first example of a second-order phase transition far away from thermal equilibrium," *Z. Phys.*, vol. 237, no. 1, pp. 31-46, 1970.

[58] H. Haken, "Cooperative phenomena in systems far from thermal equilibrium and in nonphysical systems," *Rev. Mod. Phys.*, vol. 47, no. 1, pp. 67-121, 1975.

[59] M. Corti and V. DeGiorgio, "Analogy between the laser and second-order phase transitions: Measurement of "coexistence curve" and "susceptibility" for a single-mode laser near threshold," *Phys. Rev. Lett.*, vol. 36, no. 20, pp. 1173-1176, 1976.

[60] A. Gatti and L. Lugiato, "Quantum images and critical fluctuations in the optical parametric oscillator below threshold," *Phys. Rev. A*, vol. 52, no. 2, pp. 1675-1690, 1995.

[61] A. P. Kazantsev, S. G. Rautian, and G. I. Surdutovich, "Theory of a gas laser with nonlinear absorption," *Sov. Phys. JETP*, vol. 27, no. 5, pp. 756-762, 1968.

[62] A. P. Kazantsev and G. I. Surdutovich, "The quantum theory of the laser," *Sov. Phys. JETP*, vol. 29, no. 6, pp. 1075-, 1969.

[63] R. Salomaa and S. Stenholm, "Gas laser with saturable absorber. I. Single-mode characteristics," *Phys. Rev. A*, vol. 8, no. 5, pp. 2695-2711, 1973.

[64] R. Salomaa, "Field fluctuations in bistable gas lasers," *J. Phys. A*, vol. 7, no. 9, pp. 1094-1116, 1974.

[65] J. F. Scott, M. Sargent III, and C. D. Cantrell, "Laser-phase transition analogy: Application to first-order transitions," *Opt. Commun.*, vol. 15, no. 1, pp. 13-16, 1975.

[66] A. Baczynski, A. Kossakowski, and T. Marszalek, "Quantum theory of dye lasers," *Z. Phys. B*, vol. 23, no. 2, pp. 205-212, 1976.

[67] R. B. Schaefer and C. R. Willis, "Quantum-mechanical theory of the organic-dye laser," *Phys. Rev. A*, vol. 13, no. 5, pp. 1874-1890, 1976.

[68] P. H. Lee, P. B. Schoefer, and W. B. Barker, "Single-mode power from a 6328Å laser incorporating neon absorption," *Appl. Phys. Lett.*, vol. 13, no. 11, pp. 373-375, 1968.

[69] H. M. Gibbs, S. L. McCall, and T. N. C. Venkatesan, "Differential gain and bistability using a sodium-filled Fabry-Perot interferometer," *Phys. Rev. Lett.*, vol. 36, no. 19, pp. 1135-1138, 1976.

[70] S. Ruschin and S. H. Bauer, "Bistability, hysteresis and critical behavior of a CO_2 laser, with SF_6 intracavity as a saturable absorber," *Chem. Phys. Lett.*, vol. 66, no. 1, pp. 100-103, 1979.

[71] J. W. Won, "Optical bistabilities, phase transitions, and Q-switch characteristics of an N_2O laser with a saturable NH_3 absorber," *Opt. Lett.*, vol. 8, no. 2, pp. 79-81, 1983.

[72] L. A. Lugiato, P. Mandel, S. T. Dembinski, and A. Kossakowski, "Semiclassical and quantum theories of bistability in lasers containing saturable absorbers," *Phys. Rev. A*, vol. 18, no. 1, pp. 238-254, 1978.

[73] S. T. Dembinski, A. Kossakowski, L. A. Lugiato, and P. Mandel, "Semiclassical and quantum theory of the bistability in lasers containing saturable absorbers. II," *Phys. Rev. A*, vol. 18, no. 3, pp. 1145-1151, 1978.

[74] P. Mandel and T. Erneux, "Stationary, harmonic, and pulsed operations of an optically bistable laser with saturable absorber. I," *Phys. Rev. A*, vol. 30, no. 4, pp. 1893-1901, 1984.

[75] T. Erneux and P. Mandel, "Stationary, harmonic, and pulsed operations of an optically bistable laser with saturable absorber. II," *Phys. Rev. A*, vol. 30, no. 4, pp. 1902-1909, 1984.

[76] R. Roy, "Photon distributions of lasers with first-order phase-transition analogies," *Phys. Rev. A*, vol. 20, no. 5, pp. 2093-2104, 1979.

[77] J. F. Scott, "Laser-phase transition analogy: Tricritical points," *Opt. Commun.*, vol. 15, no. 3, pp. 343-344, 1975.

[78] M. Mortazavi and S. Singh, "Tricritical behavior in the laser with a saturable absorber," *Phys. Rev. Lett.*, vol. 64, no. 7, pp. 741-744, 1990.

[79] M. Mortazavi, F. Rawwagah, and S. Singh, "Measurements of intensity fluctuations in a laser with a saturable absorber," *Phys. Rev. A*, vol. 65, no. 2, pp. 025803, 2002.

[80] P. Mandel, "Lasers with saturable absorber driven by a coherent field," *Z. Phys. B*, vol. 33, no. 2, pp. 205-209, 1979.

[81] G. S. Agarwal and S. Dattagupta, "Higher-order phase transitions in systems far from equilibrium: Multicritical points in two-mode lasers," *Phys. Rev. A*, vol. 26, no. 2, pp. 880-887, 1982.

[82] G. S. Agarwal, "Existence of multistability in systems with complex order parameters," *Phys. Rev. A*, vol. 26, no. 2, pp. 888-891, 1982.

[83] P. Mandel and F.-K. Fang, "Lasers with two-photon saturable absorbers," *Phys. Lett. A*, vol. 82, no. 2, pp. 59-61, 1981.

[84] G. P. Agrawal, "Lasers with three-level absorbers," *Phys. Rev. A*, vol. 24, no. 3, pp. 1399-1403, 1981.

[85] P. Mandel, "On the transition from absorptive to dispersive behavior of a laser due to nonlinear losses," *Phys. Lett. A*, vol. 83, no. 5, pp. 207-210, 1981.

[86] M. D. Lukin, M. Fleischhauer, M. O. Scully, and V. L. Velichansky, "Intracavity electromagnetically induced transparency," *Opt. Lett.*, vol. 23, no. 4, pp. 295-297, 1998.

[87] R.-H. Rinkleff and A. Wicht, "The concept of white light cavities using atomic phase coherence ," *Phys. Scri.*, vol. T118, pp. 85-88, 2005.

[88] A. Wicht, K. Danzmann, M. Fleischhauer, M. Scully, G. Müller, and R.-H. Rinkleff, "White-light cavities, atomic phase coherence, and gravitational wave detectors," *Opt. Commun.*, vol. 134, no. 1-6, pp. 431-439, 1997.

[89] G. G. Karapetyan, "The increase of gravitational-wave interferometer sensitivity by employing stochastic resonance mechanism in nonlinear white-light cavity," *Opt. Commun.*, vol. 238, no. 1-3, pp. 35-43, 2004.

[90] S. Wise, G. Mueller, D. Reitze, D. B. Tanner, and B. F. Whiting, "Linewidth-broadened Fabry-Perot cavities within future gravitational wave detectors," *Class. Quantum Grav.*, vol. 21, no. 5, pp. S1031-S1036, 2004

[91] M. S. Shahriar, G. S. Pati, R. Tripathi, V. Gopal, M. Messall, and K. Salit, "Ultrahigh enhancement in absolute and relative rotation sensing using fast and slow light," *Phys. Rev. A*, vol. 75, no. 5, pp. 053807, 2007.

[92] A. Rocco, A. Wicht, R.-H. Rinkleff, and K. Danzmann, "Anomalous dispersion of transparent atomic two- and three-level ensembles," *Phys. Rev. A*, vol. 66, no. 5, pp. 053804, 2002.

[93] A. Wicht, R.-H. Rinkleff, L. S. Molella, and K. Danzmann, "Comparative study of anomalous dispersive transparent media," *Phys. Rev. A*, vol. 66, no. 6, pp. 063815, 2002.

[94] B. R. Mollow, "Power spectrum of light scattered by two-Level systems," *Phys. Rev.*, vol. 188, no. 5, pp. 1969-1975, 1969.

[95] C. Szymanowski, A. Wicht, and K. Danzmann, "On negative dispersion without absorption in bichromatically driven two-level systems," *J. Mod. Opt.*, vol. 44, no. 7, pp. 1373-1392, 1997.

[96] H. Friedmann and A. D. Wilson-Gordon, "Enhanced index of refraction in a population-trapped three-level system," *Opt. Commun.*, vol. 98, no. 4-6, pp. 303-308, 1993.

[97] L. J. Wang, A. Kuzmich, and A. Dogariu, "Gain-assisted superluminal light propagation," *Nature*, vol. 406, pp. 277-279, 2000.

[98] A. Dogariu, A. Kuzmich, and L. J. Wang, "Transparent anomalous dispersion and superluminal light-pulse propagation at a negative group velocity," *Phys. Rev. A*, vol. 63, no. 5, pp. 053806, 2001.

[99] R. Fleischhaker and J. Evers, "Four-wave mixing enhanced white-light cavity," *Phys. Rev. A*, vol. 78, no. 5, pp. 051802(R), 2008.

[100] A. A. Savchenkov, A. B. Matsko, and L. Maleki, "White-light whispering gallery mode resonators," *Opt. Lett.*, vol. 31, no. 1, pp. 92-94, 2006.

[101] A. M. Steinberg and R. Y. Chiao, "Dispersionless, highly superluminal propagation in a medium with a gain doublet," *Phys. Rev. A*, vol. 49, no. 3, pp. 2071-2075, 1994.

[102] G. S. Pati, R. Tripathi, M. Messall, K. Salit, and M. S. Shahriar, "Controllable anomalous dispersion and group index nulling via bi-frequency raman gain in Rb vapor for application to ultraprecision rotation sensing," e-print arXiv: quant-ph/0512260.

[103] G. S. Pati, M. Salit, K. Salit, and M. S. Shahriar, "Demonstration of a tunable-bandwidth white-light interferometer using anomalous dispersion in atomic vapor," *Phys. Rev. Lett.*, vol. 99, no. 13, pp. 133601, 2007.

[104] K. Wodkiewicz and M. S. Zubairy, "Effect of laser fluctuations on squeezed states in a degenerate parametric amplifier," *Phys. Rev. A*, vol. 27, no. 4, pp. 2003-2007, 1983.

[105] S. Sultana and M. S. Zubairy, "Effect of finite bandwidth on refractive-index enhancement and lasing without inversion," *Phys. Rev. A*, vol. 49, no. 1, pp. 438-448, 1994.

[106] *Selected Papers on Noise and Stochastic Process*, N. Wax, Ed. New York: Dover, 1954.

[107] J. von Neumann, *Mathematical Foundations of Quantum Mechanics*. Princeton, NJ: Princeton University Press, 1955.

[108] A. N. Korotkov, "Continuous quantum measurement of a double dot," *Phys. Rev. B*, vol. 60, no. 8, pp. 5737-5742, 1999.

[109] H. Mabuchi and P. Zoller, "Inversion of quantum jumps in quantum optical systems under continuous observation," *Phys. Rev. Lett.*, vol. 76, no. 17, pp. 3108-3111, 1996.

[110] M. A. Nielsen and C. M. Caves, "Reversible quantum operations and their application to teleportation," *Phys. Rev. A*, vol. 55, no. 4, pp. 2547-2556, 1997.

[111] M. Ueda and M. Kitagawa, "Reversibility in quantum measurement processes," *Phys. Rev. Lett.*, vol. 68, no. 23, pp. 3424-3427, 1992.

[112] A. Imamoḡlu, "Logical reversibility in quantum-nondemolition measurements," *Phys. Rev. A*, vol. 47, no. 6, pp. R4577-R4580, 1993.

[113] A. Royer, "Reversible quantum measurements on a spin 1/2 and measuring the state of a single system," *Phys. Rev. Lett.*, vol. 73, no. 7, pp. 913-917, 1994.

[114] Y.-S. Kim, Y.-W. Cho, Y.-S. Ra, and Y.-H. Kim, "Reversing the weak quantum measurement for a photonic qubit," *Opt. Express*, vol. 17, no. 14, pp. 11978-11985, 2009.

[115] M. Ueda, N. Imoto, and H. Nagaoka, "Logical reversibility in quantum measurement: General theory and specific examples," *Phys. Rev. A*, vol. 53, no. 6, pp. 3808-3817, 1996.

[116] M. Ban, "Probabilistically reversible measurements," *J. Phys. A*, vol. 34, no. 45, pp. 9669-9676, 2001.

[117] M. Koashi and M. Ueda, "Reversing measurement and probabilistic quantum error correction," *Phys. Rev. Lett.*, vol. 82, no. 12, pp. 2598-2601, 1999.

[118] N. Katz, M. Neeley, M. Ansmann, R. C. Bialczak, M. Hofheinz, E. Lucero, A. O'Connell, H. Wang, A. N. Cleland, J. M. Martinis, and A. N. Korotkov, "Reversal of the weak measurement of a quantum state in a superconducting phase qubit," *Phys. Rev. Lett.*, vol. 101, no. 20, pp. 200401, 2008.

[119] A. N. Korotkov and A. N. Jordan, "Undoing a weak quantum measurement of a solid-state qubit," *Phys. Rev. Lett.*, vol. 97, no. 16, pp. 166805, 2006.

[120] T. Di, A. Muthukrishnan, M. O. Scully, and M. S. Zubairy, "Quantum teleportation of an arbitrary superposition of atomic Dicke states," *Phys. Rev. A*, vol. 71, no. 6, pp. 062308, 2005.

[121] A. S. Parkins, P. Marte, P. Zoller, and H. J. Kimble, "Synthesis of arbitrary quantum states via adiabatic transfer of Zeeman coherence," *Phys. Rev. Lett.*, vol. 71, no. 19, pp. 3095-3098, 1993.

[122] A. S. Parkins, P. Marte, P. Zoller, O. Carnal, and H. J. Kimble, "Quantum-state mapping between multilevel atoms and cavity light fields," *Phys. Rev. A*, vol. 51, no. 2, pp. 1578-1596, 1995.

[123] S. Stenholm and K.-A. Suominen, *Quantum Approach to Informatics*. Hoboken, NJ: John Wiley & Sons, 2005.

[124] J. Martin, B. W. Shore, and K. Bergmann, "Coherent population transfer in multilevel systems with magnetic sublevels. III. Experimental results," *Phys. Rev. A*, vol. 54, no. 2, pp. 1556-1569, 1996.

[125] W. Lange and H. J. Kimble, "Dynamic generation of maximally entangled photon multiplets by adiabatic passage," *Phys. Rev. A*, vol. 61, no. 6, pp. 063817, 2000.

[126] B. Wang, Y. Han, J. Xiao, X. Yang, C. Zhang, H. Wang, M. Xiao, and K. Peng, "Preparation and determination of spin-polarized states in multi-Zeeman-sublevel atoms," *Phys. Rev. A*, vol. 75, no. 5, pp. 051801(R), 2007.

VITA

Name: Qingqing Sun

Address: Department of Physics and Astronomy,
Texas A&M University, College Station, TX 77843

Email Address: qsun@physics.tamu.edu

Education: B.S., Physics, Peking University, 2001

M.S., Physics, Peking University, 2004

Publications:

(1) Q. Sun, Y. V. Rostovtsev, J. P. Dowling, M. O. Scully, and M. S. Zubairy, *Phys. Rev. A* 72, 031802 (R) (2005).

(2) Q. Sun, Y. V. Rostovtsev, and M. S. Zubairy, *Phys. Rev. A* 74, 033819 (2006).

(3) C. H. R. Ooi, Q. Sun, M. S. Zubairy, and M. O. Scully, *Phys. Rev. A* 75, 013820 (2007).

(4) Q. Sun, P. Hemmer, and M. S. Zubairy, *Phys. Rev. A* 75, 065803 (2007).

(5) Q. Sun, M. Al-Amri, Ali Kamli and M. S. Zubairy, *Phys. Rev. A* 77, 062501 (2008).

(6) Q. Sun, M. Selim Shahriar and M. S. Zubairy, *Phys. Rev. A* 78, 013805 (2008).

(7) Q. Sun, M. Al-Amri, and M. S. Zubairy, *Phys. Rev. A* 78, 043801 (2008).

(8) Q. Sun, H. Nha, and M. S. Zubairy, *Phys. Rev. A* 80, 020101 (R) (2009).

(9) Q. Sun, M. Al-Amri, and M. S. Zubairy, *Phys. Rev. A* 80, 033838 (2009).